Biomass-derived porous carbonaceous materials and their composites as adsorbents for cationic and anionic dyes: A review

Mohammad M. Hassan[1,*], Christopher M. Carr[2]

[1] *Bioproduct and Fiber Technology Team, AgResearch Limited, 1365 Springs Road, Lincoln, Christchurch 7674, New Zealand.*

[2] *The Clothworkers' Center for Textile Materials Innovation for Healthcare, University of Leeds, Leeds LS2 5JQ, United Kingdom.*

Abstract

The dyes currently used in the textile industry are not highly toxic or carcinogenic, but some dyes and their degradation products may have some levels of toxicity. The intense color of the effluent obstructs the photosynthesis reaction affecting the viability of aquatic plants, animals and organisms. Various classes of dyes are used in the textile dyehouses depending on fiber types, but the water-soluble dyes are problematic. Of the remediation processes investigated, the adsorption process is attractive because of the low cost and versatility. Carbonaceous adsorbents and their composites have grabbed much attention because of their very high dye-binding capacity. In this review, the characteristics of effluents coming from dyehouse treating various fibers have been discussed. The potential of biomass-based

[*] Corresponding author: Tel.: +64-3-321-8755, fax: +64-3-321-8811

E-mail: mahbubul.hassan@agresearch.co.nz

feedstocks to produce carbonaceous adsorbents and the application of the produced adsorbents for the removal of various types of dyes from effluent have been compiled and critically reviewed. The effect of preparation conditions on the surface area, porosity, pore volume, and chemical characteristics of the produced carbonaceous adsorbents has been outlined and discussed. The dye-binding capacities of various carbonaceous adsorbents at the optimum conditions have been compiled. Moreover, the dye-binding mechanisms and dye sorption isotherm models of various carbonaceous adsorbents are discussed. The analysis of the compiled dye-adsorption data shows that some carbonaceous adsorbents derived from biomasses and their composites can be serious competitors for the traditional coal and petroleum-derived activated carbons (ACs). The pore volume and functional groups of dyes are the deciding factors in achieving high dye adsorption.

Keywords: Biomass-derived carbon adsorbents; dyehouse effluent; decolorization; water-soluble dyes; adsorption; isotherm models

1. Introduction

Textile chemical processing industries are at the crossroads because of many unprecedented issues. One of them is the strict consent limits set by environmental agencies, which considerably increased the processing cost of textiles due to the extra-cost incurring for the treatment of effluent (Hassan and Hawkyard, 2002a). Textile coloration industry effluent poses a great threat to the environment, especially in some developing countries as it is polluting watercourses limiting the availability of clean drinking water in those countries. The pollution caused by the textile coloration industries cannot be hidden because of the

intense color of the discharged effluent, which is persistent due to the poor biodegradability of these dyes. Sometimes the dyes used in the textile industry may not be highly toxic or carcinogenic as the production of such a type of dyes has been ceased by the leading dye manufacturers. However, some dyes have some level of toxicity, and the degradation products of them could be more harmful compared to the dyes themselves because of the formation of the more toxic compounds. The acute toxicity tests against microcrustacean, *Daphnia similis*, showed that the degradation products of dyes were more toxic than the parent dyes (Lambert and Davy, 2011). Moreover, the discharged effluents containing high concentrations of dyes, sizing agents, salts, textile auxiliaries, and finishing agents to water streams increase the turbidity of water and obstruct the photosynthesis reactions, resulting in oxygen deficiency and jeopardizing the viability of aquatic animals and plants (da Silva Leite et al., 2016). Many synthetic dyes are complexed with toxic heavy metals, such as copper, chromium, and nickel, to enhance their brightness and colorfastness to washing. When these dyes are degraded, these toxic heavy metals are released to the environment, contaminating the watercourses, which may end up in the food webs and food chains. Except for polyester, most of the fibers are dyed with water-soluble dyes that pose greater risks compared to the water-insoluble non-ionic disperse dyes used in polyester fiber dyeing. Of the dyes used in industry, anionic reactive, acid, direct, and cationic basic dyes are problematic because of their high water-solubility as they are not removed by the primary treatments.

Waste materials are ideal feedstock for the development of carbonaceous adsorbents as many of them are rich in carbon. Their application as a feedstock to produce adsorbents not only valorize them but also eliminates the waste disposal problems. Various biomass-based feedstocks, such as agricultural wastes, house-hold waste, industrial waste, have been investigated for the manufacturing of AC, biochar, graphene, carbon nanotubes (CNT), and

other carbonaceous adsorbents. However, only very few of them are used for the commercial production of adsorbents because of the difficulty to get enough quantity of a certain feedstock and the involved cost to collect and transport economic quantities for commercial production.

Several reviews have been published in the area of removal of dyes from effluent (Hassan and Carr, 2018; Yagub et al., 2014; Karcher et al., 2002), but none of them specifically addressed the removal of water-soluble dyes from dyehouse effluent by biomass-derived carbonaceous adsorbents and their composites, did not study the effect of processing conditions on the characteristics of the produced carbonaceous adsorbents, and compared dye-binding capacities of dyes by carbonaceous adsorbents and their dye-binding mechanisms. Moreover, some of them are old and in the meantime, many high-performing adsorbents have been developed for the removal of dyes. In this review, characteristics effluent coming from dyehouses that process various types of fibers, and various types of biomass feedstocks investigated to produce carbonaceous adsorbents have been discussed. The optimum conditions for adsorption by various carbon adsorbents and their maximum dye-binding capacities, their dye-binding mechanisms are compiled, critically reviewed, and the future directions of dye adsorbent development are outlined.

2. Characteristics of effluent from dyehouse processing various fibers

2.1. Cellulosic fiber

For the manufacturing of woven fabrics, various sizing agents including starch, polyvinyl alcohol (PVA), and carboxymethylcellulose are applied to warp yarns, and they are removed before dyeing preferably by enzymatic treatments. They are also pre-treated with a cocktail of strong alkali, detergents, and wetting agents at a boil to remove oils, fats, and other contaminants, to improve their wettability and to enable uniform dyeing (Hassan and Hawkyard, 2002b). In some cases, the fabric is also bleached using hydrogen peroxide at a boil. The most popular class of dyes used for the dyeing of cellulosic fibers is reactive dyes. Therefore, cellulosic processing industry effluent contains sizing materials, wetting agents, detergents, enzymes, hemicellulose, alkali, salts, and dyes.

2.2. Protein fiber

Animal fibers contain fat, suint, and minerals, and these are removed from fibers by the scouring treatment in an aqueous solution of a non-ionic detergent, a wetting agent, and a dispersing agent at 60 °C. Sometimes pesticides are used on animals (especially on lambs and sheep) to protect them from flystrike and they end up in the scouring effluent. The detergents used in animal fiber scouring are mainly non-ionic based-on nonylphenol ethoxylate (NPEO), a known endocrine inhibitor (Ahel et al., 1994a; Ahel et al., 1994a). It was reported that male fish exposed to NPEOs had lower testicular weight, lower fertility, and decreased survival of young fishes (Soares et al., 2008). Wool fibers are frequently treated with chlorine and a polyamide resin to make them shrink-proof. The most popular classes of dyes for the dyeing of protein fibers are acid and reactive dyes. Therefore, animal fiber processing industry effluent contains fats, detergents, resins, chlorine, pesticides, salt, acid and reactive dyes, and dyeing auxiliaries.

2.3. Synthetic fiber

Synthetic fiber processing effluent is comparatively clean as no sizing agent is used for the weaving of synthetic fiber-made textiles. Of the synthetic fibers, polyester fibers are dyed with water-insoluble disperse dyes. The level of exhaustion of dyes into the fiber is so high that any treatment of effluent is redundant. Acrylic fibers are dyed with basic dyes and therefore the effluent coming from the acrylic fiber dyeing industry contains mainly basic dyes and auxiliary chemicals. Polyamide fibers (such as nylon fiber) are dyed with mainly acid dyes and therefore the effluent produced contains acid dyes and several dyeing auxiliaries. All fibers and fabrics are undergone with various chemical finishing processes and therefore the dyehouse effluent not only contains dyes but also contains salt, various dyeing auxiliaries, starch, PVA, and finishing agents that may interfere with dye adsorption by carbonaceous adsorbents.

3. Biomass feedstocks for carbonaceous adsorbents

Because of low cost and abundant availability, biomass-based feedstocks became popular to produce carbonaceous adsorbents. They can be classified into the following categories:

3.1. Plant and crop residues

Plant and crop residues remaining after harvesting could be an excellent feedstock to produce carbonaceous adsorbents. They are composed of cellulose, hemicellulose, and lignin that may include stems, leaves, and roots. These are abundantly available feedstock to produce carbonaceous adsorbents that don't compete with food crops for arable land. The investigated crop residue-based feedstocks are rice stalk and husk (Liu et al., 2016), wheat straw (Li et al., 2016; Han et al., 2018), rice straw (Sangon et al., 2018), weeds (Güzel et al., 2017), bamboo (Yang et al., 2014), corn stover and cobs (Fang, 2012), cassava (Beakou et al., 2017a; Beakou et al., 2017b), swiss grass (Mahmoud et al., 2016), sugarcane bagasse pith (Amin, 2008), jute fiber (Senthilkumar et al., 2006), and sorghum stalk (Khalil et al., 2017). They are quite low-density feedstock and therefore the yield is low.

3.2. Tree and fruit residues

They are a byproduct of the forest and wood processing industries, such as waste timber, lignin, sawdust, shavings, off-cuts, trims, and wood pulp. These are a major source of biomass for carbonaceous adsorbent production. They are of comparatively higher density than the crop residues, low value, and a waste product. The forest residues, such as Ashe juniper wood (Choi et al., 2019), wood waste (Kelm et al., 2019), poplar catkins (Liu et al., 2017a), lignin (Hayashi et al., 2000), and sawdust (Dos Santos et al., 2016; Gan et al., 2004), have been studied as a carbonaceous adsorbent precursor. The investigated fruit waste feedstocks may include orange peel (Bayrak and Uzgör, 2013; Galán et al., 2013), pine cone (Özhan et al., 2014; Dawood et al., 2017), coconut shell (Gupta and Khatri, 2019; Zheng et al., 2017; Islam et al., 2017; Senthilkumaar et al., 2006; Furlan et al., 2010; Lee et al., 2006), coconut flower (Senthilkumaar et al., 2006), Brazilian pine fruit shell (Calvete et al., 2010;

Cardoso et al., 2011), coconut coir (Sharma et al., 2010), coir pith and almond shell (Thitame and Shukla), cocoa pod husk (Bellow et al., 2011), coffee waste (Dos Santos et al., 2015), pomegranate peel (Ahmad et al., 2014), carob (Sayğili and Güzel, 2018), date palm rachis (Daoud et al., 2017), *Persea americana* nut (Regti et al., 2017), mangosteen skin (Hong et al., 2017), and macadamia shell (Du et al., 2017).

3.3. Animal and fishery waste

They are mostly of proteinous materials and fat harvested from slaughtering houses, and fish processing industries. They are waste products and therefore could be a cheap carbon feedstock. Various animal and fishery waste investigated as a feedstock for the manufacturing of AC may include animal manure (Li et al., 2018), crab shell (Dai et al., 2018), leather hide shavings (Huang et al., 2018), scallop (Shirzad-Siboni et al., 2014), fishery waste (Fadhil et al., 2017; Marrakchi et al., 2017b), marine shell (Hopkins and Hawboldt, 2020) and fish scales (Achieng et al., 2019). Most of them are usually thrown out but they are rich in elemental carbon and nitrogen, which may positively affect the carbon yield.

3.4. Municipal organic solid wastes

These biomasses may include organic house-hold waste and similar commercial, industrial and institutional wastes. They could be various types, oil and fat, used textiles, organic solvents, food waste, paper, and cardboard packaging, etc. The accumulated municipal organic solid wastes have caused a series of environmental issues including the uncontrolled

release of greenhouse gases. These wastes usually go to landfills but there is a shortage of landfills for waste disposal, which made the waste management system non-sustainable. Their use as a feedstock for carbonaceous adsorbent production will solve the waste disposal issues and will limit contamination of lands. The studied feedstocks may include laundry sewage sludge (Silva et al., 2016), textile sludge (Sonai et al., 2016), waste scrap tire Tuzen et al., 2018), cotton denim waste Silva et al., 2018), refined olive pumice oil (Marrakchi et al., 2017b), refuse-derived fuel (Nagano et al., 2000), coffee residue (Jung et al., 2017), municipal sewage sludge Guo et al., 2017, cellulose carbamate (Zhou et l., 2017), and sucrose (Galán et al., 2013).

3.5. Marine and freshwater biomasses

They may include aquatic photosynthetic eukaryotic organisms, such as microscopic unicellular microalgae (e.g. chlorella, diatoms, etc.) to macroscopic multicellular organisms (such as giant kelp, phytoplankton, and brown alga). They produce oxygen in the aquatic environment and contain chlorophyll pigment produced by photosynthesis but lack a sterile covering of cells around their reproductive cells. These photosynthetic organisms have several advantages over land-based plants, such as higher yields, do not need arable land for production, and utilize nutrients from water/wastewater without competing for fertilizers with food crops (Brune et al., 2009). The microalgae investigated to produce carbonaceous adsorbents may include *Spirulina platensis* (Nautiyal et al., 2016)), *chlorella sp.* (Chang et al., 2015), *Sargassum longifolium* and *Hypnea valentiae* (Aravindhan et al, 2009), *Gelidium sesquipedale* (Ferrera-Lorenzo et al., 2014), and *Enteromorpha prolifera* (Sun et al., 2013).

4. Types of carbonaceous adsorbents

Various types of carbonaceous adsorbents, such as biochar, AC, graphite, graphene, and CNTs, have been investigated for the decolorization of dyehouse effluents. Fig. 1 shows the feedstocks, activation methods, and modifications investigated for the manufacturing of various carbonaceous adsorbents.

Fig. 1. Feedstocks, activation methods, and modifications investigated for the manufacturing of various carbonaceous adsorbents from biomasses.

4.1. Biochar

Biochar is a porous, cheap, and carbon-rich black product produced by pyrolyzing biomasses. Biochar initially received attention for the carbon sequestration, soil fertility enhancement (Novak et al., 2009), bio-oil and bioenergy production (Gaunt and Lehmann, 2008), and environmental remediation through the disposal of solid waste (Mohan et al., 2014). However, their application has already been realized for the removal of heavy metals (Qian et al., 2016), and dyes from potable water and effluent (Dai et al., 2018). Biochar prepared from different feedstocks, such as Ashe juniper (*Juniperus ashei*) (Choi et al., 2019), pine cone (Dawood et al., 2017), cassava waste (Beakou et al., 2017a), wheat straw (Li et al., 2016), switchgrass (Mahmoud et al., 2016), wood waste (Kelm et al., 2019), etc., have been investigated for the removal of dyes from dyehouse effluent. Biochar derived from chicken bone, rice husk, and other feedstocks modified with magnetic nanoparticles by

embedding Fe_2O_3 nanoparticles into the AC particles (Akbarnezhad and Safa, 2018; Oladipo et al., 2017; Han et al., 2015), and CNTs (Inyang et al. 2014), also has been investigated for the same purpose. Not only biochar prepared by the carbonization method used for the removal of dyes from their effluent but also biochar prepared by the hydrothermal method has also been investigated for the same purpose (Islam et al., 2017).

236236

4.1.1. Manufacturing of biochar

Biochar is manufactured by using the similar methods used for the manufacturing of AC or by hydrolytic method, but carbonization is usually carried out under the air environment. The process starts with the drying of the biogenic materials in a woven at 60–90 °C and then chopping into small pieces. The chopped pieces are slowly heated, and pyrolysis and gasification of the chopped biomass are carried out in a furnace at 400 to 1000 °C under the nitrogen atmosphere followed by slow cooling. The organic compound of the biomass is broken down into methyl ester, methyl indole, oxalic acid, acetic acid, and volatile gasses. Mainly three kinds of products are produced, gaseous volatiles, liquid oily compound, and black solids. The residue left is mainly carbon with small organic residues, which is ground to a fine powder by a milling machine. To achieve high carbon content, the feedstock needs to be pyrolyzed at 1000 °C or over, which is possible if the carbon content of the feedstock is high but for agriculture residues, pyrolysis is carried out at below 700 °C (even 300 °C) to increase the biochar yield and also to preserve the mechanical properties of the biomass to ease grinding (Weber and Quicker, 2018). The produced biochar becomes porous due to the release of the volatiles. The pore size and chemical characteristics of the produced biochar depend on the type of feedstocks used, pyrolysis temperature, rate of heating, and residence time in the furnace. To enhance their adsorption capability, biochar is chemically activated by

treating with strong acids or modified by in situ production of magnetic nanoparticles. Strong acids, alkali, and salts are used as an activating agent. Chemical activation induces the formation of pores and increases the surface area of the produced biochar. Fig. S1 (Supplementary Material) shows the SEM micrographs of a biochar precursor, golden shower (GS), and biochar derived from it by carbonization (GSB) and also by hydrolytic oxidation (GSH). The produced biochar was activated by impregnating in K_2CO_3 followed by pyrolysis at 800 °C (Tran et al., 2018). It is evident that before chemical activation, the precursor and the biochar produced by the hydrolytic method hardly had any pores but after the chemical activation, they became highly porous, and their BET surface area reached 1413 and 1238 m^2/g respectively.

Table 1. Adsorption conditions and adsorption capacity of various anionic dyes by biochar derived from various feedstocks.

4.1.2. Dye binding capacity of activated and modified biochar

Table 1 shows the dye-binding capacities of various anionic and cationic dyes by the activated and modified biochar, and also conditions used to assess their dye-binding performance. Of them, CNT-modified biochar showed a very poor dye-binding capacity for the C.I. Basic Blue 9 (6.2 mg/g), a cationic dye. Rice husk-derived AC showed moderate removal of C.I. Basic Violet 10 (96.5 mg/g) and C.I. Acid Orange (98.5 mg/g), respectively. Conversely, some of the activated biochar showed excellent removal of dyes, such as the biochar derived from crab shell showed a dye-binding capacity of 12502 and 20317 mg/g for the removal of cationic C.I. Basic Green 4 and anionic C.I. Direct Red 28 dyes respectively. Leather shaving derived biochar produced at 900 °C also showed excellent binding of C.I.

Direct Red 28. However, the leather shavings contain chromium which is used as a tanning agent, and its hexavalent form is a carcinogen. Biochar is equally effective for the removal of anionic and cationic dyes. Magnetic modification of biochar eases their recovery from the treated water but had a seriously detrimental effect on their dye adsorption capacity.

4.1.3. Merits and demerits of biochar as a dye adsorbent

Biochar-based adsorbents are quite cheap as the feedstocks used for their manufacturing are various wastes and they are prepared by carbonizing at lower temperatures compared to the AC. The high dye-binding capacity of cationic and anionic dyes and cheaper production costs may make them a serious contender to replace AC adsorbents.

4.2. Activated carbon

AC is a microporous carbon granule with low to the high surface area, which is the most popular adsorbent. The surface area, pore size, and surface characteristics of AC very much depend on the pyrolysis temperature, duration, and carbonization conditions. The dye adsorption capacity of AC also depends on its surface area, pore size, pore size distribution, and surface characteristics. The dye adsorption properties by carbonaceous adsorbents are greatly affected by the specific surface area and pore structure of the adsorbents (Wu et al., 2017; Li et al., 2017). Commercial AC has been investigated as adsorbents for basic, acid, and reactive dyes (Machado et al., 2011). Fig. 2 shows the typical manufacturing process of AC by a schematic diagram. AC is commercially produced from various precursors including lignocellulosic biomasses, wood, lignite, coal, coconut husk, bamboo, and

petroleum pitch by a process called gasification/carbonization. Compared to biochar production a higher carbonizing temperature is used in the case of AC production. AC has much higher carbon content compared to the biochar.

Fig. 2. Production of ACs from various types of biomasses.

4.2.1. Manufacturing

The manufacturing process is similar to biochar production but the carbonization is carried out preferably under an inert atmosphere, unlike biochar. The carbonization is a process by which various carbon-rich precursors are converted into pure carbon by heating at 600–2000 °C. Initially, the absorbed moisture and volatiles are released, and then the degradation of the surface occurs followed by the skeletal breakdown of biomass. The release of volatiles creates pores in the carbon materials. The produced carbonaceous materials still are not much porous and have a low surface area. To increase their porosity and surface area they undergo a process called activation that converts them to adsorbents (Gamby et al., 2001). The produced adsorbents are activated either by physical or by chemical activation processes. In the physical activation process, the carbonaceous materials are heated at 600–1200 °C in combination with an activating agent, such as steam, carbon dioxide, oxygen, and sulfur dioxide. Physical activation affects the pore size, pore size distribution, surface area, and oxygen content of the produced carbon. The physical activation process is simple and cheap, but the yield is compromised. The increase in activation temperature and time changes pore size distribution and increases the pore size, and surface area but also negatively affects the yield. The surface area, pore size distribution pore size and pore volume of AC are measured by nitrogen absorption test using the Brunauer–Emmett–Teller model. The higher the

nitrogen adsorption, the higher the surface area. For example, in the case of AC production from coconut shell by steam activation method showed that the nitrogen adsorption (i.e. surface area) increased with an increase in the carbonization time and temperature (Fig. S2 in Supplementary Materials). At different temperature zone, different types of reactions take place. In the conversion of wool fiber to carbon fiber, it was observed that the pore volume increased from 0.43 cm^3/g for the 300°C to 1.81 cm^3/g at 500°C (Li et al., 2008).

Fig. S3 (Supplementary Materials) shows the effect of carbonization temperature on the pore volume of AC produced from the *Arundo donax* plant (Üner and Bayrak, 2018). The pore volume increases with an increase in the carbonization temperature. The impregnation ratio also affected the formation of micropores and mesopores. In the case of 300 °C, the formation of micro and mesopores increased with an increase in the impregnation ratio of 1.5, and after which the formation of micro and mesopores started decreasing. Conversely, at 500 °C carbonization temperature, the formation of micropores decreased but the formation of mesopores increased with an increase in the impregnation ratio.

In the chemical activation process, the carbonaceous material is impregnated with a strong acid, strong base, or salt and then carbonized at much lower temperatures compared to the temperatures used for the physical activation process. Carbonaceous materials produced by carbonization is impregnated in strong acids, such as nitric acid (Moreno-Castilla et al., 2010), sulfuric acid (Kolur et al., 2019), and phosphoric acid (Yakout and El-Deen, 2016), strong bases (e.g. sodium hydroxide), and their salts such as calcium nitrate, zinc chloride, and cuprous chloride (Hu et al., 2009; Liou, 2010; Boutillara et al., 2019; Xu et al., 2019). They are then dried and then activated by heating at 450–900 °C from 1 h to 4 h under a nitrogen atmosphere. After cooling down, they are again washed with a diluted strong acid, filtered, and dried. The processing parameters, such as the activation temperature and time, types of activating agents used, impregnating ratio of carbon materials and the activating

agents, and the medium in which the activation is carryout play a great role in determining the surface area, pore volume, and pollutant adsorption capacity of the prepared AC. For example, Lua and Yang investigated the effect of chemical activation temperature on the pore size and BET surface area of AC produced from peanut shell using potassium hydroxide as a chemical activating agent, which shows that BET surface area and pore volume increased with an increase the in the activation temperature up to 800 °C but beyond that temperature the BET surface area and pore volume both decreased. Similarly, Li et al. investigated the effect of activation temperature on the surface area, degree of graphitization, lattice layer distance, and yield of the AC produced from petroleum coke using potassium hydroxide as an activating agent (Li et al., 2019) and results are tabulated in Table S1 (Supplementary Material). They found that the BET surface area, carbon content, and layer spacing of graphite increased and the degree of graphitization and yield decreased with an increase in the activation temperature.

The redox reaction of K_2CO_3 with elemental carbon of the AC during activation leads to the removal of elemental carbon which increases defects in the carbon layers (Wang et al., 2012). When the activation temperature exceeds 700 °C, the yielded potassium can intercalate into the carbon layers of AC and distort the carbon layers (Liu et al., 2015). Fig. S4 (Supplementary Material) shows the effect of activation temperature on the BET surface area and morphology of AC produced from the pistachio shell (Lua and Yang, 2004). BET surface area and micropore volume increased with an increase in activation temperature up to 800 °C and beyond that temperature both BET surface area and micropore volume started decreasing. Of the ACs investigated for the removal of reactive dyes, only the AC produced from coir pith and almond shell produced a high surface area, 1210.60 and 1133.30 m^2/g respectively. However, it was reported that the surface area of AC could be as high as 3000 m^2/g (Al-Degs et al., 2008; Hilton et al., 2012; Zhang et al., 2017).

Porous AC has many different uses and they are commercially available in two forms, granular GAC) and powdered (PAC). AC is purified and milled to powdered form with a particle diameter of a couple of hundred microns. Depending on the carbon precursors used, the apparent density of AC is ranging from 0.39 to 0.73 g/cm^3. PAC is added to the effluent as a powder by a dry feed system or as a slurry by a metering pump. After the treatment, the PAC is removed through the sedimentation process or by the filter beds during backwashing. Because of their small size, the removal of PAC from the treated effluent is cumbersome. PAC dosage could be 10 to 100 mg/L depending on the dye concentration of the effluent. On the other hand, GAC has a larger particle size compared to the PAC, which allows their separation from the treated water comparatively easy than the PAC. The diameter of GAC is between 1.2 to 1.6 mm with an apparent density between 0.4 and 0.5 g/cm^3. Instead of direct addition of GAC to effluent, they are used in the filtration column. Several factors are involved in the designing of a GAC adsorption column, such as type of GAC, surface loading rate (l/min/m^2), empty bed contact time (in min), type of contaminants and their concentration in the effluent, and carbon depth and usage. The typical empty bed contact time (EBCT) in between 10 and 15 min and the surface loading rate between 81.8 to 408.0 l/min/m^2 is effective for the removal of most of the contaminants. The effluent is pumped through the GAC filter media and clean water comes out through the outlet of the column.

4.4.2. Dye-binding capacities

In Table S2 (Supplementary Material), the reactive dye removal performance of AC produced from various biomass-based precursors are compared to several commercial ACs. Filtrasorb-400, a commercial AC produced by Calgon Carbon Corporation (USA), showed quite a high removal of C.I. Reactive Red 120 as its dye-binding capacity reached 400 mg/g

(Khraisheh et al., 2002), considerably higher compared to the AC marketed by Merck, 267.2 mg/g (Cardoso et al., 2012). AC derived from cocoa pod husk ((Bello et al., 2011), orange peel (Bayrak and Uzgör, 2013), and scallop Shirzad-Siboni et al., 2014) showed very meager level dye-binding capacity. However, AC produced from some biomasses offered considerably higher dye-binding capacity compared to even high-performing commercial ACs, such as Filtrasorb-400. For example, an AC produced from coir pith showed very high dye-binding capacity at 30 °C as high as 1791.2 and 1428.4 mg/g for the C.I. Reactive Red 2 and C.I. Reactive Yellow 145 dyes respectively, that increased to 2022.9 and 1694.3 mg/g when the dye adsorption was carried out at 60 °C ((Thitame and Shukla, 2016)). The second highest reactive dye binding was shown by the AC produced from the almond shell, which showed the C.I. Reactive Red 2 and C.I. Reactive Yellow 145A dye-binding was as high as 1639.9 and 1397.4 mg/g respectively (Thitame and Shukla, 2016). AC derived from mangosteen skin and coffee residue also showed a couple of times higher dye-binding capacity compared to the commercial ACs. The ACs derived from coconut shell had a very high surface area (2200 m^2/g) but the dye-binding performance was near to the dye-binding capacity shown by commercial Filtrasorb-400 adsorbent (Gupta and Khatri, 2019). Conversely, AC derived carbon had an even higher surface area, twice of AC derived from coir pith, but the dye-binding capacity was much lower than the AC derived from coir pith (Zhou et al., 2017), which shows that the dye-binding is not only related to the surface area of the adsorbent but also depends on other factors. The high dye-binding capacity shown by some biomass-derived ACs suggests that biomass could be an ideal feedstock for the development of high performing dye adsorbent.

4.3. Nanostructured carbon

Various nanostructured carbon, such as CNTs, graphite, and graphene, have been investigated as an adsorbent for the removal of textiles dyes from effluent. Graphite is a crystalline form of elemental carbon with its atoms arranged in a hexagonal shape. CNTs are one of the most popular and important one-dimensional (1D) nanomaterials and they could be single-walled (SWCNT) or multiwalled (MWCNT). On the other hand, graphene is a two-dimensional (2D) nanomaterial, which is an atomically thin layer of elemental carbon. Graphite oxide (Travlou et al., 2013), MWCNT (Machado et al., 2011; Dehghani et al., 2013; Ferreira et al., 2017), SWCNT (Machado et al., 2014), graphene (Liu et al., 2012; Elsagh et al., 2017), graphene oxide (Mao et al., 2020), and functionalized MWCNT (Karimifard et al., 2016), have been studied for the removal of several cationic reactive dyes.

4.3.1. Manufacturing

Currently, CNTs are synthesized by three processes: arc discharge, laser ablation, and chemical vapor deposition. Although gaseous hydrocarbons are the preferred feedstock to produce CNTs, various biomasses, such as plant materials (Xie et al., 2009), potato peel waste (Osman et al., 2019), and chitosan (Zhang et al., 2018) also have been investigated as an alternative renewable feedstock. Biomasses are also popular feedstocks to produce graphite and graphene (Das et al., 2017; Purkait et al., 2017; Sams et al., 2015). Graphene is produced by several methods including micromechanical exfoliation, liquid-phase exfoliation, chemical vapor deposition (CVD), flame synthesis, pyrolysis, and pulsed laser deposition (PLD). Of the methods investigated, the CVD method is the most popular because by this method high-quality graphene can be produced but the flame synthesis is popular for

the liquid feedstocks. It is quite difficult to produce nanostructured carbon from biomasses by pyrolysis unless a catalyst is used. Barin et al. managed to produce highly curved graphitic nanostructured carbons with a high degree of crystallinity from the hydrothermally pre-treated coconut coir dust by the pyrolysis method (Barin et al. 2014). Nickel salt was used as a catalyst to form graphitic carbon nanostructures from cellulose via pyrolysis (Sevilla and Fuertes, 2010). Biomasses are converted to graphite by a process called graphitization, which is a kind of pyrolysis, but the materials are heated above 2000 °C. However, the application of a catalyst enables graphitization at a moderately low temperature (1000 °C). Group 4-7 metals, such as Fe, Co, Mn, and Ni, are popular catalysts for the graphitization (Ōya and Marsh, 1982).

4.3.2. Dye binding capacity of CNT, and graphene

Table S3 (Supplementary Material) shows the dye-binding capacities of nanostructured carbon adsorbents. Graphene showed a quite good removal of cationic dyes as the dye-binding capacity of C.I. Basic Blue 9 at 20 °C was 153.9 mg/g, which reached 204.1 when the adsorption temperature was increased to 60 °C (Liu et al., 2012). Graphite oxide was also showed comparable dye removal as the C.I. Reactive Black 5 dye-binding capacity reached 275 mg/g when the adsorption temperature was increased to 65 °C. On the other hand, CNTs showed better dye sorption capacity compared to graphite oxide and graphene. The binding capacity of C.I. Reactive Blue 4 by SWCNT was 502.5 mg/g and MWCNT showed better dye removal than the SWCNT (Ferreira et al., 2017). Of them, graphene oxide showed the highest removal of cationic dyes as the removal of C.I. Basic Violet 1 reached 686.6 mg/g (Elsagh et al., 2017). However, some ACs derived from biomasses considerably showed a

couple of times higher dye-binding capacity compared to the nanostructured carbon adsorbents. Moreover, they are quite expensive compared to ACs.

5. Carbonaceous composite adsorbents

5.1. Carbonaceous composite adsorbents

To further increase the dye-binding capacity of carbonaceous adsorbents, they were modified with various metal doping, converting to a hydrogel and modifying with various synthetic and natural polymers. The composites of CNT with bagasse (Inyang et al., 2014), graphene oxide (GO) with chitosan and calcium alginate (Travlou et al., 2013; Guo et al., 2016; Li et al., 2013), MWCNT with xanthan gum crosslinked polyacrylic acid (Guo et al., 2018), and AC with magnesium oxide (MgO2) (Zheng et al., 2018) or alginate (Nasrullah et al., 2018), have been investigated for the removal of dyes from their aqueous solutions. Nickel nanoparticles encapsulated with C and CNT also have been studied as a dye adsorbent (Jin et al., 2018). The other composite adsorbents may include graphene sponge modified with ionic liquid (Zambare et al., 2017), heteroatom-doped AC (Liu et al., 2017), chitosan beads immobilized on AC (Filipkowska et al., 2017), GO and CNT with zeolitic imidazole framework (Abdi et al., 2017), AC/bentonite composite (Liang et al., 2017), N-doped AC (Hou et al., 2020; El-Mahdy et al., 2020), CNT/chitosan hydrogel (Goncalves et al., 2020), Zn-doped AC (Li et al., 2020), graphene-like carbon hydrogel (Yang et al., 2020), laccase immobilized on CNT (Zhang et al., 2020), lanthanide and iron-modified AC (Cheng et al., 2017), hydrochar functionalized with triethylenetetramine (TETA) (Tran et al., 2017),

AC/zeolite (Wang et al., 2018), xanthan gum-cl-poly(acrylic acid)/o-MWCNT composite hydrogel (Makhado et al., 2018), and AC/polyaniline composites (Hasan et al., 2017).

Table 2. Dye-binding performance of various modified/composite carbonaceous adsorbents studied by the batch process.

Table 2 shows the dye-binding performance of various modified and composite carbonaceous adsorbents. Of them, CNT/bagasse, and GO/chitosan composites showed very poor dye-binding capacity, which was 6.2 and 32.2 for the C.I. Basic Blue 9 (Inyang et al., 2014) and C.I. Reactive Red 120 (Guo et al., 2016) dyes respectively. However, Guo et al. achieved quite a good dye-binding capacity for the removal of C.I. Reactive Black 5 by GO/chitosan composites (Travlou et al., 2013). Laccase immobilized onto CNT also showed very poor dye-binding capacity (Zhang et al., 2020). Nickel nanoparticles encapsulated in porous carbon and carbon nanotube hybrids showed a quite good dye-binding capacity for C.I. Basic Green 4 and C.I. Direct Red 28 dyes but for other cationic and anionic dyes, the dye-binding capacity dropped to less than half of the removal achieved for the C.I. Basic Green 4 and C.I. Direct Red 28 dyes. Of the modified and composite carbonaceous adsorbents studied, graphene-like carbon hydrogel showed excellent dye removal capacity as the removal of C.I. Basic Blue 9 13381.62 mg/g (Yang et al., 2020), which is considerably better than any other carbonaceous adsorbents. On the other hand, GO/ zeolitic imidazolate framework and CNT/ zeolitic imidazolate framework composites showed a quite good dye-binding capacity which reached 3300 and 2034 mg/g for the C.I. Basic Green 4 dye respectively. The dye-binding capacity of modified AC and their composites show that they are a serious contender for the replacement of AC for the removal of dyes.

Table 2. Dye-binding performance of various modified/composite carbonaceous adsorbents studied by the batch process.

5.2. Carbonaceous material/magnetic nanoparticle composites

The high dye-binding capacity is not only enough to commercialize a dye adsorbent as the removal of adsorbents from the treated water is cumbersome. Therefore, recent research emphasized the ease of separation of adsorbent from the treated effluent resulting in the development of magnetic nanoparticles. By using a strong magnet, the used adsorbent can be easily separated from treated effluent. Magnetic nanoparticles are embedded inside the adsorbent particle or in-situ formed so that the adsorbent particles become magnetic. Mainly F_2O_3 or Fe_3O_4 nanoparticles are formed inside carbonaceous adsorbents to make them magnetic. The investigated magnetic carbonaceous carbon composites may include Fe3O4 embedded biochar (Akbarnezhad and Safa, 2018), chicken bone-derived (CBD) biochar (Oladipo et al., 2017), rice-husk derived RHD) biochar (Han et al., 2015), AC (Saroyan et al., 2017), GO/MWCNT (Long et al., 2017), reduced GO (Sharif et al., 2017), CNT (Duman et al., 2016), graphene/polypyrrole (PPy) composite (Bai et al., 2015), carboxyl functionalized GO (CO-f-GO) (Guo et al., 2018), dodecyl sulfate GO (DDS-f-GO (Yakout and Shaker, 2016), PAC (Jafari et al., 2016), AC (Kyzas et al., 2014), and AC derived from *Nigella sativa L.* waste (AC-NS) (Abdel-Ghani et al., 2019).

Table 3. Adsorption of anionic and cationic dyes by magnetic AC adsorbents studied by the batch process.

Table 3 shows the dye-binding capacity of magnetic carbonaceous adsorbents. Of the magnetic nanoparticles investigated, only a few of them show some levels of potential as adsorbents. Magnetic AC good reactive dye removal as the dye-binding capacity reached 445.3 mg/g (Saroyan et al., 2017), but still was very inferior to even unmodified biochar and AC. Magnetic Fe_3O_4-modified biochar derived from chicken bone showed poor cationic dye removal capacity, 96.5 mg/g (Duman et al., 2016. Magnetic CNT-Fe_3O_4 nanocomposite and magnetic CNT-κ-carrageenan-Fe_3O_4 nanocomposite showed very poor dye-binding capacity and the maximum removal was achieved at highly acidic conditions (pH 2), which is not favorable as the pH of the effluent will need to be reduced to that level by using strong acids and after the dye removal again will need to raise the pH to neutral by adding alkali. They are not practical for the removal of dyes as the cost of production of these adsorbents will be relatively high and the levels of removal achieved are only one-third of the dye-binding capacity shown by AC. The challenges of magnetic nanoparticles are the non-availability of these adsorbents at an economical price, low reactive dye-binding capacity, poor decolorization efficiency, and the economic regeneration of the adsorbents.

6. Dye adsorption process

The dye adsorption process involves the dye-binding mechanism, the factors affecting the dye sorption process, and dye sorption isotherm and adsorption kinetics.

6.1. Dye binding mechanisms

The understanding of the dye-binding on carbonaceous adsorbent is crucial for the designing of a dyehouse effluent treatment plant. The functional groups of carbonaceous materials play an important role in the adsorption of dyes on these adsorbents. The biochar has surface acidic groups (hydroxyl, carboxyl, and phenolic groups) that are formed by thermal decomposition of the hemicellulose, cellulose, and lignin of the biomasses (Mohan et al., 2015), which may provide active sites for the binding of cationic basic dyes. Therefore, the biochar shows better cationic dye sorption capacity compared to anionic acid, reactive and direct dyes (Liu et al., 2017b). Little is known about the nature of the anion exchange sites on biochar surfaces and the pH-independent oxygen-containing functional groups contribute anion exchange sites in biochar (Lawrinenko and Laird, 2015).

The dye-binding mechanism of AC could be quite complex as the dye-binding could be physical and or chemical adsorption. Depending on the activation processes and carbonization temperatures used, they may have anionic hydroxyl, carboxyl, and sulfonate groups (Mao et al., 2020; Pengthamkeerati and Satapanajaru, 2015; Tessmer et al., 1997). Depending on the dye classes, the dye-binding mechanism of carbonaceous adsorbents could be different as different dyes have different functional groups. Fig. 3 shows the dye-binding mechanisms of cationic dyes by various carbonaceous adsorbents. Cationic dyes have amino, or quaternary ammonium cationic groups but may also have hydroxyl and hydrophobic methyl functional groups enabling their binding by electrostatic bonding, hydrogen bonding, or Van der Waal's force, and π–π stacking, as shown in Fig. 3.

Fig. 3. Mechanism of binding of C.I. Basic Blue 9 (BB) and C.I. Basic Violet 3 (BV) with AC (left) and CNT (right) respectively.

The mechanisms of binding of anionic dyes by AC and CNTs are shown in Fig. 4. Direct, acid, and reactive dyes are anionic as they have sulfonate groups that confer their water solubility. Unmodified AC also can bind anionic dyes by hydrogen bonding and π–π stacking but that types of bonds are weak compared to the electrostatic bonding. ACs are porous and when dye molecules pass through them, the dye molecules simply trapped inside the porous structure of the AC irrespective of the ionic character of the dye. Therefore, the adsorption of dyes by AC could be described as a combined physical and chemical adsorption. However, to enhance the anionic dye removal capacity of carbonaceous adsorbents, cationic amino groups are introduced in ACs by nitration followed by amination (Abe et al., 2000; Mahaninia et al., 2015), so that they can electrostatically bind anionic dyes.

Fig. 4. Binding mechanism of anionic C.I. Acid Blue 25 (AB), C.I. Reactive Blue 4 (RB) and C.I. Reactive Red 2 (RR) dyes with AC (left) and CNT (right).

In the case of graphene and CNTs, not only surface functional groups of them but also the defects of their surface also play a great role in binding dye molecules. CNTs are composed of graphene or graphitic sheets rolled up into a cylindrical shape and possess a π-conjugative structure with a highly hydrophobic surface (Rajabi et al., 2017). Depending on the functional groups on the surface of graphene and CNTs, dye molecules can be attached to them by ionic interactions, π-π stacking, van der Waal's force, and hydrogen bonding individually or simultaneously. Aberration corrected transmission electron microscopy, X-ray photoelectron spectroscopy, and the density functional studies revealed that oxygen-containing hydroxyl and epoxy functional groups are distributed in the form of the island (Shin et al., 2017).

6.2. Factors affecting dye sorption

The conditions at which dye adsorption is carried out determines the final dye sorption capacity of AC. The dye sorption is affected by various factors, such as the pH, temperature, concentration of dyes in the effluent, and the chemical structure of dyes.

6.2.1. Effect of pH on dye sorption capacity

It is necessary to identify the optimum pH at which the maximum dye adsorption takes place for a particular carbonaceous adsorbent. In the case of dye binding by electrostatic interaction, the pH of dye solution plays a great role in the dye sorption and the maximum dye sorption occurs at the pH at which the affinity between the adsorbent and the dye molecules are the highest. The maximum affinity can be identified by measuring the zeta potential of the adsorbent. To absorb the cationic dye, the carbonaceous material will need to be negatively charged or for the binding of anionic dyes, the adsorbent will need to be positively charged. In the case of dye binding by Van der Waal's force, hydrogen bonding, or hydrophobic-hydrophobic interaction, the pH of the effluent may not play a great role and adsorption occurs at wider pHs. The optimum pH for dye binding by AC varies depending on the activation processes used and also on the carbon precursors types. Depending on the precursors and activation process used, the optimum pH of reactive dye removal by AC could be 1–6. Table 1 shows that in the case of biochar, the maximum binding of cationic basic dye occurred at neutral to the alkaline side of the pH (except the CI. Basic Green 4 adsorption by biochar derived from *Manihot esculenta* Crantz waste) but the anionic direct, reactive and acid dyes were favorably removed at the acidic side of the pH. The zeta potential measurement of biochar derived from various agricultural wastes (straw of wheat, rice, corn,

fava bean, soybean, peanut, rice hull, etc.) shows that the negative charge of biochar increased with an increase in the pH from 2.5 to 7.0, suggesting the increase of cationic dye-binding capacity with an increase in the dye solution pH (Yuan et al., 2017). On the other hand, Qi et al. reported that the biochar derived from wood shaving and combusted wood shaving, and AC showed an increase in positive charge at pH below 5.7, 7.3, and 6.0 respectively, i.e. the anionic dyes are adsorbed at those pHs and the cationic dyes are absorbed above those pHs (Qi et al., 2017). Fig. S5 (Supplementary Material) shows the effect of pH on the binding capacities of various cationic and anionic dyes by carbonaceous adsorbents. The binding of cationic and anionic dyes is favored at the alkaline and acidic side of the pH respectively. It was found that AC produced from the almond shell, coir pith, sawdust, textile sludge, and pomegranate peel showed the highest anionic dye-binding capacity at pH 1–2. On the other hand, the AC produced from marine algae, pine-fruit shell, and scallop showed the highest removal as high as pH 6. The adsorption capacity of AC is increased if the adsorption is carried out at a relatively high temperature, which is not desirable as it will increase the energy cost of the treatment. The installation costs of AC-based filtrations are not expensive, and they show the best hydrodynamic properties and can be easily regenerated.

6.2.2. Effect of temperature

The temperature at which the adsorption is carried out also plays a great role in the dye adsorption capacities of carbonaceous materials. The reaction of dye molecules with carbonaceous adsorbents could be endothermic or exothermic. The diffusion and binding of dye molecules into carbonaceous adsorbents occurs due to the constant thermal motion of atoms, and molecules depending on the energy available. The temperature increase provides

heat energy, which increases the molecular motion of dye molecules and drives their diffusion into the adsorbent.

6.2.3. Effect of dye concentration

The dye adsorption capacity also depends on the concentration of dyes in the effluent. If the dye concentration is too low, the dye adsorption may not reach the saturation point and the adsorbent will be underused. The dye adsorption capacity increases with an increase in the concentration of dye in the effluent up to the point of saturation of dye binding sites of the adsorbent beyond which no increase in dye-binding capacity is observed as the dye-binding sites are fully occupied by the dye molecules. Conversely, the dye adsorption efficiency decreases with an increase in the concentration of dye in the effluent because of the saturation of the adsorption sites on the surface of the adsorbent. Travlou et al found that the removal of C.I. Reactive Black 5 by graphite oxide increased from 205–275 mg/g when the adsorption temperature was increased from 25 to 65 °C (Travlou et al., 2013). Similarly, the binding capacity of C.I. Basic Blue 9 by graphene increased from 153.9 to 204.1 mg/g when the adsorption temperature was increased from 20 to 60 °C (Liu et al., 2012).

Table 4. Chemical structure and molecular weight of several basic and reactive dyes.

6.2.4. Effect of functional groups of dyes

The functional groups (especially the number of ionic groups), molecular weight, and the substituent groups of dyes play a great role in the dye-binding capacities of various textile dyes. Low molecular weight dyes are readily absorbed into carbonaceous adsorbents compared to the high-molecular-weight dyes. Table 4 shows the chemical structure of dyes

with their molecular weight. In the removal of reactive dyes by a commercial AC (Supelco) it was found that the dye-binding capacity for the C.I. Reactive Blue 2 was 4.9 mg/g but for the C.I. Reactive Yellow 2 was only 3.17 mg/g. Both of them have a similar number of sulfonate groups but the molecular weight of the former dye was lower compared to the later dye (Low and Lee, 1997). The molecular weight of C.I. Reactive Blue and C.I. Reactive Red 23 are nearer and also have a similar number of anionic sulfonate groups but the presence of the diethylene group in the C.I. Reactive Red 2 drastically reduced its adsorption into the Supelco adsorbent. Sun et al. observed that in the removal of three reactive dyes by AC derived from marine algae, C.I. Reactive Blue 4 showed the highest dye-binding capacity and C.I. Reactive Blue 4 (M_w 681.39) dye-binding capacity was almost double of the dye-binding capacity observed for the C.I. Reactive Blue 171 (M_w 1418.93) (Sun et al., 2013). Although the later dye had a triple number of anionic sulfonate groups than the former dye, the molecular weight of the later dye was more than double of the former dye, which restricted its adsorption into the adsorbent. In the case of AC derived from coir pith and almond shell, in both cases, lower molecular weight reactive dye (C.I. Reactive Red 2, M_w=615.34) showed higher dye-binding capacity than the higher molecular weight reactive dye (C.I. Reactive Yellow 145, M_w=1026.25) although the higher molecular weight dye had double anionic groups compared to the lower molecular weight dye (Thitame and Shukla, 2016). In the case of the removal of C.I. Basic Blue 9 and C.I. Basic Violet 3 dyes by biochar derived from corn cob, it was found that the former dye showed higher removal compared to the latter. The former three amino groups and the later had three dimethyl quaternary ammonium groups. The presence of dimethyl groups in the later dye considerably reduced its removal by the biochar, which suggests that the substituent groups of a dye also affect the dye-binding capacity of carbonaceous adsorbents.

6.2.5. Effect of pore volume of adsorbent

The pore volume of adsorbent plays a great role in the adsorption of dyes as the pore volume allows the binding of the highest number of dye molecules to it. Al-Degs et al. studied the effect of the surface area of microporous and mesoporous AC on the adsorption of several reactive dyes from solution (Al-Degs et al., 2004). They found that the correlation between the surface area of AC and the dye adsorption is quite poor, rather the adsorption of dyes is better related to their pore volume (Al-Degs et al., 2004). It was reported that when the pore size of a porous material is smaller than 1.7 times the size of the adsorbate molecule, the repulsion between the adsorbate molecules significantly increases resulting in requiring higher adsorption energies (Lawrence, 2014). The most effective pore sizes are in the range of 1.7–6 times of the adsorbate molecule size (Branton and Bradley, 2010). Therefore, not the surface area of the adsorbents but their pore volume governs the dye sorption.

6.3. Dye adsorption isotherm and kinetic modeling

6.3.1. Dye adsorption isotherm models

The adsorption of anionic and cationic dyes by carbonaceous adsorbents can be expressed by various isotherm models, but the most common are Langmuir, Freundlich, Temkin, and Liu models. They are important tools to understand the distribution of dye molecules at the solid adsorbent and the liquid phases at equilibrium. Adsorption isotherms are used to describe the dye molecule interaction with the carbonaceous adsorbent, adsorption equilibrium, and the dye-binding active sites of the adsorbents (Cao et al., 2014). Adsorption isotherm expresses the amount of adsorbate on the carbonaceous adsorbent surface as a function of its concentration at a constant temperature. They are used to predict the adsorption capacities of a dye by a particular carbonaceous adsorbent and also to fit the

experimental equilibrium data. A comparison of the R^2 values obtained from the adsorption models indicates which model provides the best fit for the adsorption of dyes by the carbonaceous adsorbents.

The Langmuir model is based on four assumptions: all of the adsorption sites are equivalent, and each site can only accommodate one molecule, the surface is energetically homogeneous and adsorbed molecules do not interact, there are no phase transitions, and at the maximum adsorption, only a monolayer is formed (Langmuir, 1916). The Langmuir model presumes constant adsorption energy and independent of surface coverage. When a monolayer of dye molecules covers the adsorption surface, maximum adsorption is observed. Adsorption only occurs on localized sites on the surface, not with other adsorbates. The linear form of the Langmuir model can be represented as:

$$\frac{C_e}{q_e} = \frac{1}{q_m K_L} + \frac{C_e}{q_m} \qquad [1]$$

where q_e represents equilibrium dye concentration on carbonaceous adsorbent (mg/g), C_e represents equilibrium dye concentration in solutions (mg/L), K_L is the Langmuir adsorption constant (L/mg) and q_m is the complete monolayer adsorption capacity (mg/g). The separation factor R_L can identify the favorability of the adsorption process, which can be calculated by the following formula:

$$R_L = \frac{1}{1+K_L C_i} \qquad [2]$$

Where $R_L = 1$ suggests linear adsorption, $R_L = 0$ irreversible adsorption, $0<R_L<1$ favorable adsorption, and $R_L>1$ unfavorable adsorption.

According to the Freundlich model, adsorption takes place at the heterogeneous surfaces of varied affinities. The linear form of this model is represented as (Freundlich, 1906):

$$\ln q_e = \ln K_F + \frac{1}{n} \ln C_e \qquad (1)$$

where K_F (l/g) and n (dimensionless) are Freundlich isotherm constants which represent the adsorption and the degree of nonlinearity between solution concentration and adsorption, respectively. A plot of ln q_e vs ln C_e would result in a straight line with a slope of $1/n$ and intercept of ln K_F. The Temkin isotherm model, like the Freundlich model, is one of the earliest isotherm models, which was developed to describe the adsorption of hydrogen atom onto platinum electrodes in an acidic aqueous solution. In the Temkin adsorption isotherm equation, the energy of adsorption is a linear function of surface coverage. This adsorption model is only valid for medium ion concentrations. The linear form of the model is as follows (Vijayaraghavan et al., 2006):

$$q_e = \frac{Rt}{b} \ln K_T + \frac{RT}{b} \ln C_e \qquad (2)$$

where b is a Temkin constant which is related to the heat of sorption (J/mol) and K_T is a Temkin isotherm constant (l/mg) (Samarghandi et al., 2009).

The adsorption of reactive dyes by AC can be described by using Freundlich and Langmuir models. For example, the adsorption of reactive dyes by AC mainly is represented by the Langmuir isotherm model and the kinetic data usually follows the pseudo-second-order model. Dos Santos *et al.* found that adsorption of C.I. Reactive Orange 107 onto AC made from sawdust followed the Langmuir model (Dos Santos et al., 2016). In the removal of C.I. Reactive Blue 19 by the AC produced from sewage sludge by carbonizing at 750 °C, Silva et al. found that the adsorption followed the isothermal parameters of the Freundlich model, but the kinetic data followed the pseudo-second-order model (Silva et al., 2016). For example, Fig. S6 (Supplementary Materials) shows Freundlich, Langmuir, and Temkin isotherm models for the adsorption of C.I. Reactive Yellow 145 onto AC derived from the almond shell and coir pith (Thitame and Shukla, 2016). It was reported that the adsorption of a cationic dye (C.I. Basic Blue 9) by graphene adsorbent can be described by the Langmuir

isotherm model (Liu et al., 2012). It was reported that the adsorption of a cationic and an anionic dye by activated carob derived from coconut husk followed the Langmuir and Freundlich isotherm models (Aljeboree et al., 2017). Liu et al. developed a new model for the adsorption of heavy metals by microbial aggregates, known as aerobic granules, which is a combination of Langmuir and Freundlich isotherm models by eliminating the monolayer assumptions of the Langmuir model and the infinite adsorption assumption of the Freundlich model (Liu et al., 2003). The Liu model predicts that all the active sites of the adsorbent cannot have the same energy. In the linear, form the equation can be expressed as:

$$lnQ_e/(Q_{th}^e - Q_e) = n \ln C_e - \ln K_{ads} \quad (9)$$

Values of K_{ads} and n can be easily determined from the slope and intercept of Eq. 9. Liu isotherm model can also be is utilized to describe the adsorption of anionic dyes by AC and magnetic AC adsorbents as shown in Fig. 5.

Fig. 5. Isotherm models of adsorption of C.I. Reactive 120 and dyes removed by AC (a) and magnetic-AC (d). Reproduced with permission from refs. (Cardoso et al., 2012; Liu et al., 2019).

6.3.2. Kinetic models

Kinetic models are utilized to determine the mechanism of the sorption process including the rate of adsorption, diffusion control, and mass transfer. Depending on the rate of adsorption, reaction kinetics could be first order and second order. Legergen proposed a first-order rate of reaction to describe the kinetic process of liquid-solid phase adsorption of oxalic

acid and malonic acid onto charcoal (Lee et al., 1986), which is probably the first model to describe the rate of adsorption. The equation as:

$$\frac{d(q_t)}{dt} = k_1 (q_e - q_t) \qquad (9)$$

Where q_e and q_t are the amounts of dye adsorbed (mg/g) at the equilibrium and at the time t (min), respectively, and k_1 is the pseudo-first-order rate constant (/min). If the eq. 1 is integrated with the boundary conditions of $q_t = 0$ at t=0 and $q_t=q_t$ at t=t, then the equation can be written as:

$$\ln\left(\frac{q_e}{q_e - q_t}\right) = k_1 t \qquad (10)$$

By rearranging equations 1 and 2, the pseudo-first-order equation can be expressed as

$$\log(q_e - q_t) = \log q_e - \frac{k_1}{2.303} t \qquad (11)$$

In 1995, a new kinetic model was proposed to describe the kinetics of divalent metal ion uptake onto peat as the uptake followed the second-order of reaction (Rodríguez et al., 2009). The equation can be written as:

$$\frac{dq_t}{dt} = k_2 (q_e - q_t)^2 \qquad (12)$$

where q_e and q_t are the numbers of active sites occupied at the equilibrium and at the time t (min), respectively, and k_2 is the pseudo-second-order rate constant (g/mg/min). If the eq. 11 is integrated with the boundary conditions of $q_t = 0$ at t=0 and $q_t=q_t$ at t=t and rearranging, the

$$\frac{t}{q_t} = \frac{1}{k_t q_e^2} + \frac{1}{q_e} \qquad (13)$$

where k_2 is the pseudo-second-order rate constant (g/mol/min), and the initial sorption rate (h) is equal to $k_t q_e^2$ (g/mol/min). These two equations are mostly used to describe the adsorption of reactive dyes by various adsorbents. For example, it was reported that the adsorption of basic dyes by thermochemically activated carbonaceous adsorbent showed the pseudo-second-order adsorption model (Fig. 6).

Fig. 6. Pseudo-second-order kinetic models the removal of C.I. Basic Blue 9 (Methylene Blue) and C.I. Basic Green 4 (Malachite Green) by thermochemically activated carbonaceous material. Reproduced with permission from ref. (Gupta and Khatri, 2019).

7. Conclusions and future directions

The carbonaceous adsorbent development in the last decade mainly emphasized the enhancement of dye-binding capacity by novel activation methods, development of carbon hydrogel, and composite carbon adsorbents. However, the dye-binding mechanisms of the carbonaceous adsorbents remained the same as the conventional ACs. The carbonaceous adsorbent preparation conditions show great effects on the surface area, porosity, pore volume, chemical characteristics, and dye-binding capacity of the produced carbon adsorbents. It is not the greater surface area of the adsorbent but its pore volume governs the high adsorption of dyes. Some of the biomass-derived carbonaceous adsorbents may become a serious competitor for the commercially available coal and petroleum-derived conventional ACs as they exhibited a couple of times higher dye-binding capacity compared to the

conventional ACs. For example, the graphene-like carbon hydrogel showed excellent cationic dye-binding capacity, 13381.62 mg/g, compared to the commercial Filtrasorb-400 AC. As the removal of carbon particles from treated effluent is cumbersome, recent research emphasized the development of magnetic carbonaceous adsorbents by embedding magnetic nanoparticles (mostly Fe_3O_4) into the carbonaceous adsorbent particles. However, the magnetic modification of carbonaceous adsorbent drastically reduced their dye adsorption capacity as the porosity of the adsorbent decreased. The magnetic modification may not be necessary as the carbon adsorbent can be easily separated from the treated water by suspension or secondary filtration. The dye-binding capacity is affected by the molecular weight, the number of ionic groups, and the presence of other substituent groups of the dye. There is a strong correlation between the dye-binding capacity and the pore volume of the carbonaceous adsorbent.

The modification of carbonaceous materials that increases the pore volume of the adsorbent and the introduction of high-charge ionic functional groups will need to be further researched and optimized to achieve the highest adsorption capacity. Almost in all of the dye adsorption studies used only dye solutions instead of a real dyehouse effluent but the actual dyeing effluent contains salt, starch, and various dyeing auxiliaries, other than the dyes and these admixtures may compete with dye molecules in the adsorption of dyes and may bind to the adsorbents reducing the sites available for anchoring dye molecules. Therefore, future studies for the development of dye adsorbents should use real dyehouse effluent for their adsorption studies or at least needs to study the effect of these admixtures in effluent on the dye adsorption behavior.

Declaration of Competing Interest

The authors declare that they have no known competing financial interests or personal relationships that could have appeared to influence the work reported in this paper.

Supplementary Material

Supplementary material associated with this article can be found, in the online version.

References

Abdel-Ghani, N.T., El-Chaghaby, G.A., Rawash, E.A., Lima, E.C., 2019. Magnetic activated carbon nanocomposite from Nigella sativa L. waste (MNSA) for the removal of Coomassie brilliant blue dye from aqueous solution: Statistical design of experiments for optimization of the adsorption conditions. J. Adv. Res. 17, 55–63.

Abdi, J., Vossoughi, M., Mahmoodi, N.M., Alemzadeh, I., 2017. Synthesis of metal-organic framework hybrid nanocomposites based on GO and CNT with high adsorption capacity for dye removal. Chem. Eng. J. 326, 1145–1158.

Abe, M., Kawashima, K., Kozawa, K., Sakai, H., Kaneko, K., 2000. Amination of activated carbon and adsorption characteristics of its aminated surface. Langmuir 16, 5059–5063.

Achieng, G.O., Kowenje, C.O., Lalah, J.O., Ojwach, S.O., 2019. Preparation, characterization of fish scales biochar and their applications in the removal of anionic indigo carmine dye from aqueous solutions. Water Sci. Technol. 80, 2218–2231.

Ahel, M., Giger, W., Koch, M., 1994a. Behavior of alkylphenol polyethoxylate surfactants in the aquatic environment – I Occurrence and transformation in sewage treatment. Water Res. 28, 1131–1142.

Ahel, M., Giger, W., Schaffner, C., 1994b. Behavior of alkylphenol polyethoxylate surfactants in the aquatic environment – II Occurrence and transformation in rivers. Water Res., 28, 1143–1152.

Ahmad, M.A., Puad, N.A.A., Bello, O.S., 2014. Kinetic, equilibrium and thermodynamic studies of synthetic dye removal using pomegranate peel activated carbon prepared by microwave-induced KOH activation. Water Resour. Ind. 6, 18–35.

Akbarnezhad, A.A., Safa, F., 2018. Biochar-based magnetic nanocomposite for dye removal from aqueous solutions: response surface modeling and kinetic study. Russian J. Appl. Chem. 91, 1856–1866.

Al-Degs, Y. S., El-Barghouthi, M.I., Khraisheh, M.A., Ahmad, M.N., Allen, S.J., 2004, Effect of Surface Area, Micropores, Secondary Micropores, and Mesopores Volumes of Activated Carbons on Reactive Dyes Adsorption from Solution. Separat. Sci. Technol. 39, 97–111.

Al-Degs, Y.S., El-Barghouthi, M.I., El-Sheikh, A.H., Walker, G.M., 2008. Effect of solution pH, ionic strength, and temperature on adsorption behavior of reactive dyes on activated carbon. Dyes Pigment. 77, 16–23.

Aljeboree, A.M., Alshirifi, A.N., Alkaim, A.F., 2017. Kinetics and equilibrium study for the adsorption of textile dyes on coconut shell activated carbon. Arabian J. Chem. 10, S3381–S3393.

Amin, N.K., 2008. Removal of reactive dye from aqueous solutions by adsorption onto activated carbons prepared from sugarcane bagasse pith. Desalination 223, 152–161.

Aravindhan, R., Raghava Rao, J., Unni Nair, B., 2009. Preparation and characterization of activated carbon from marine macro-algal biomass. J. Hazard. Mater. 162, 688-694.

Bai, L., Li, Z., Zhang, Y., Wang, T., Lu, R., Zhou, W., Gao, H., Zhang, S., 2015. Synthesis of water-dispersible graphene-modified magnetic polypyrrole nanocomposite and its

ability to efficiently adsorb methylene blue from aqueous solution. Chem. Eng. J. 279, 757–766.

Barin, G.B., de Fátima Gimenez, I., da Costa, L.P., Filho, A.G.S., Barreto, L.S., 2014. Influence of hydrothermal carbonization on formation of curved graphite structures obtained from a lignocellulosic precursor. Carbon 78, 609–612.

Bayrak, Y., Uzgör, R., 2013. Removal of reactive dye from aqueous solution by activated carbon. Asian J. Chem. 25, 71–78.

Beakou, B.H., El Hassani, K., Houssaini, M.A., Belbahloul, M., Oukani, E., Anouar, A., 2017a. A novel biochar from Manihot esculenta Crantz waste: Application for the removal of Malachite Green from wastewater and optimization of the adsorption process. Water Sci. Technol. 76, 1447–1456.

Beakou, B.H., El Hassani, K., Houssaini, M.A., Belbahloul, M., Oukani, E., Anouar, A., 2017b. Novel activated carbon from Manihot esculenta crantz for removal of methylene blue. Sust. Environ. Res. 27, 215–222.

Bello, O.S., Ahmad, M.A., Siang, T.T., 2011. Utilization of cocoa pod husk for the removal of Remazol Black B reactive dye from aqueous solutions: Kinetic, equilibrium and thermodynamic studies. Trend. Appl. Sci. Res. 6, 794–812.

Boutillara, Y., Tombeur, J.L., De Weireld, G., Lodewyckx, P., 2019. In-situ copper impregnation by chemical activation with $CuCl_2$ and its application to SO_2 and H_2S capture by activated carbons. Chem. Eng. J. 372, 631–637.

Branton, P., Bradley, R.H., 2010. Effects of active carbon pore size distributions on adsorption of toxic organic compounds. Adsorption 17, 293–301.

Brune, D.E., Lundquist, T.J., Benemann, J.R., 2009. Microalgal biomass for greenhouse gas reductions: Potential for replacement of fossil fuels and animal feeds. J. Environ. Eng. 135, 1136–1144.

Calvete, T., Lima, E.C., Cardoso, N.F., Vaghetti, J.C., Dias, S.L., Pavan, F.A., 2010. Application of carbon adsorbents prepared from Brazilian-pine fruit shell for the removal of reactive orange 16 from aqueous solution: Kinetic, equilibrium, and thermodynamic studies. J. Environ. Manag. 91, 1695–706.

Cao, C., Xiao, L., Chen, C., Shi, X., Cao, Q., Gao, L., 2014. In situ preparation of magnetic Fe_3O_4/chitosan nanoparticles via a novel reduction–precipitation method and their application in adsorption of reactive azo dye. Powder Technol. 260, 90–97.

Cardoso, N.F., Lima, E.C., Royer, B., Bach, M.V., Dotto, G.L., Pinto, L.A.A., Calvete, T., 2012. Comparison of Spirulina platensis microalgae and commercial activated carbon as adsorbents for the removal of Reactive Red 120 dye from aqueous effluents. J. Hazard. Mater. 241–242, 146–153.

Cardoso, N.F., Pinto, R., Lima, E.C., Pinto, I.S., 2011. Removal of Remazol Black B textile dye from aqueous solution by adsorption. Desalination 269, 92–103.

Choi, J., Won, W., Capareda, S.C., 2019. The economical production of functionalized Ashe juniper derived-biochar with high hazardous dye removal efficiency. Ind. Crop. Prod. 137, 672–680.

Chang, Y.-M., Tsai, W.-T., Li, M.-H., 2015. Characterization of activated carbon prepared from chlorella-based algal residue. Bioresour. Technol. 184, 344–348.

Cheng, S., Zhang, L., Xia, H., Peng, J., 2017. Characterization and adsorption properties of la and Fe modified activated carbon for dye wastewater treatment. Green Proc. Syn. 6, 487–498.

Choi, J., Won, W., Capareda, S.C., 2019. The economical production of functionalized Ashe juniper derived-biochar with high hazardous dye removal efficiency. Ind. Crop. Prod. 137, 672–680.

Dai, L., Zhu, W., He, L., Tan, F., Zhu, N., Zhou, Q., He, M., Hu, G., 2018. Calcium-rich biochar from crab shell: An unexpected super adsorbent for dye removal, Bioresour. Technol. 267, 510–516.

Daoud, M., Benturki, O., Kecira, Z., Girods, P., Donnot, A., 2017. Removal of reactive dye BEZAKTIV Red S-MAX) from aqueous solution by adsorption onto activated carbons prepared from date palm rachis and jujube stones. J. Mol. Liquid. 243, 799–809.

da Silva Leite, L., de Souza Maselli, B., de Aragão Umbuzeiro, G., Pupo Nogueira, R.F., 2016. Monitoring ecotoxicity of disperse red 1 dye during photo-Fenton degradation. Chemosphere 148, 511–517.

Das, V.K., Shifrina, Z.B., Bronstein, L.M., 2017. Graphene and graphene-like materials in biomass conversion: Paving the way to the future. J. Mater. Chem. A 5, 25131–25143.

Dawood, S., Sen, T.K., Phan, C., 2017. Synthesis and characterization of slow pyrolysis pinecone biochar in the removal of organic and inorganic pollutants from aqueous solution by adsorption: Kinetic, equilibrium, mechanism and thermodynamic. Bioresour. Technol. 246, 76–81.

Dehghani, M.H., Naghizadeh, A., Rashidi, A., Derakhshani, E., 2013. Adsorption of Reactive Blue 29 dye from aqueous solution by multiwall carbon nanotubes. Desal. Water Treat. 51, 7655–7662.

Dos Santos, D.C., Adebayo, M.A., Lima, E.C., Pereira, S.F.P., Cataluña, R., Saucier, C., Thue, P.S., Machado, F.M., 2015. Application of carbon composite adsorbents prepared from coffee waste and clay for the removal of reactive dyes from aqueous solutions. J. Braz. Chem. Soc. 26, 924–938.

Dos Santos, J.M., Felsner, M.L., Almeida, C.A.P., Justi, K.C., 2016. Removal of Reactive Orange 107 dye from aqueous solution by activated carbon from Pinus elliottii sawdust: A response surface methodology study. Water Air Soil Pollut. 227, 300.

Du, C., Xue, Y., Wu, Z., Wu, Z., 2017. Microwave-assisted one-step preparation of macadamia nut shell-based activated carbon for efficient adsorption of Reactive Blue. New J. Chem. 41, 15373–15383.

Duman, O., Tunç, S., Bozoğlan, B.K., Polat, T.G., 2016. Removal of triphenylmethane and reactive azo dyes from aqueous solution by magnetic carbon nanotube-κ-carrageenan-Fe_3O_4 nanocomposite. J. Alloy. Compound. 687, 370–383.

El-Mahdy, A.F.M., Liu, T.-E., Kuo, S.-W., 2020, Direct synthesis of nitrogen-doped mesoporous carbons from triazine-functionalized resol for CO_2 uptake and highly efficient removal of dyes. J. Hazard. Mater. 391, 122163.

Elsagh, A., Moradi, O., Fakhri, A., Najafi, F., Alizadeh, R., Haddadi, V., 2017. Evaluation of the potential cationic dye removal using adsorption by graphene and carbon nanotubes as adsorbents surfaces. Arab. J. Chem. 10, S2862-S2869.

Fadhil, A.B., Ahmed, A.I., Salih, H.A., 2017. Production of liquid fuels and activated carbons from fish waste. Fuel 187, 435–445.

Fang, R., 2012. Preparation of corncob-based biochar and its application in removing basic dyes from aqueous solution. Adv. Mater. Res. 550–553, 2420–2423.

Ferrera-Lorenzo, N., Fuente, E., Suárez-Ruiz, I., Ruiz, B., 2014. KOH activated carbon from conventional and microwave heating system of a macroalgae waste from the Agar-Agar industry. Fuel Process. Technol. 121, 25–31.

Ferreira, G.M.D., Hespanhol, M.C., de Paula Rezende, J., dos Santos Pires, A.C., Gurgel, L.V.A., da Silva, L.H.M., 2017. Adsorption of red azo dyes on multi-walled carbon nanotubes and activated carbon: A thermodynamic study. Colloids and Surfaces A: Physicochem. Eng. Asp. 529, 531–540.

Filipkowska, U., Jóźwiak, T., Szymczyk, P., Kuczajowska-Zadrożna, M., 2017. The use of active carbon immobilized on chitosan beads for RB5 and BV10 dye removal from aqueous solutions. Prog. Chem. Appl. Chitin Deriv. 22, 14–26.

Freundlich, H.M.F., 1906. Over the adsorption in solution. J. Phys. Chem. 57, 385–471.

Furlan, F.R., de Melo da Silva, L.G., Morgado, A.F., de Souza, A.A.U., Guelli Ulson de Souza, S.M.A., 2010. Removal of reactive dyes from aqueous solutions using combined coagulation/flocculation and adsorption on activated carbon. Resour. Conserv. Recycl. 54, 283–290.

Galán, J., Rodríguez, A., Gómez, J.M., Allen, S.J., Walker, G.M., 2013. Reactive dye adsorption onto a novel mesoporous carbon. Chem. Eng. J. 219, 62–68.

Gamby, J., Taberna, P.L., Simon, P., Fauvarque, J.F., Chesneau, M., 2001. Studies and characterizations of various activated carbons used for carbon/carbon supercapacitors. J. Power Sour. 101, 109−116.

Gan, Q., Allen, S.J., Matthews, R., 2004. Activation of waste MDF sawdust charcoal and its reactive dye adsorption characteristics. Waste Manag. 24, 841–848.

Gaunt, J.L., Lehmann, J., 2008. Energy balance and emissions associated with biochar sequestration and pyrolysis bioenergy production. Environ. Sci. Technol., 42, 4152–4158.

Gonçalves, J.O., da Silva, K.A., Rios, E.C., Crispim, M.M., Dotto, G.L., de Almeida Pinto, L.A., 2020. Chitosan hydrogel scaffold modified with carbon nanotubes and its application for food dyes removal in single and binary aqueous systems. Int. J. Biologic. Macromol. 142, 85–93.

Guo, R., Jiao, T., Li, R., Chen, Y., Guo, W., Zhang, L., Zhou, J., Zhang, Q., Peng, Q., 2018. Sandwiched Fe_3O_4/carboxylate graphene oxide nanostructures constructed by layer-by-

layer assembly for highly efficient and magnetically recyclable dye removal. ACS Sust. Chem. Eng., 6, 1279–1288.

Guo, T., Yao, S., Chen, H., Yu, X., Wang, M., Chen, Y., 2017. Characteristics and adsorption study of the activated carbon derived from municipal sewage sludge. Water Sci. Technol., 76, 1697–1705.

Guo, X., Qu, L., Tian, M., Zhu, S., Zhang, X., Tang, X., Sun, K., 2016. Chitosan/graphene oxide composite as an effective adsorbent for reactive red dye removal. Water Environ. Res. 88, 579–588.

Gupta, K., Khatri, O.P., 2019. Fast and efficient adsorptive removal of organic dyes and active pharmaceutical ingredient by microporous carbon: Effect of molecular size and charge. Chem. Eng. J. 378, 122218.

Güzel, F., Sayğili, H., Akkaya Sayğili, G., Koyuncu, F., Yılmaz, C., 2017. Optimal oxidation with nitric acid of biochar derived from pyrolysis of weeds and its application in removal of hazardous dye methylene blue from aqueous solution. J. Cleaner Prod. 144, 260–265.

Han, L., Xue, S., Zhao, S., Yan, J., Qian, L., Chen, M., 2015. Biochar supported nanoscale iron particles for the efficient removal of methyl orange dye in aqueous solutions. PLoS One 10, e0132067.

Han, X., Wang, H., Zhang, L., 2018. Efficient removal of methyl blue using nanoporous carbon from the waste biomass. Water Air Soil Pollut. 229, 26.

Hassan, M.M., Carr, C.M., 2018. A critical review on recent advancements of the removal of reactive dyes from dyehouse effluent by ion-exchange type adsorbents. Chemosphere 209, 201–219.

Hassan, M.M., Hawkyard, C.J., 2002a. Reuse of spent dyebath following decolorization with ozone. Col. Technol. 118, 104–111.

Hassan, M.M., Hawkyard, C.J., 2002b. Decolorization of effluent with ozone and re-use of spent dyebath. In: Christie, R.M. (ed.), Environmental Aspects of Textile Dyeing, Elsevier, Chichester, United Kingdom.

Hayashi, J., Kazehaya, A., Muroyama, K., Watkinson, A.P., 2000. Preparation of activated carbon from lignin by chemical activation. Carbon 38, 1873–1878.

Hilton, R., Bick, P., Tekeei, A., Leimkuehler, E., Pfeifer, P., Suppes, G.J., 2012. Mass balance and performance analysis of potassium hydroxide activated carbon. Industrial Eng. Chem. Res. 51, 9129–9135.

Hong, X., Fang, C., Tan, M., Zhuang, H., Liu, W., Hui, K.S., Ye, Z., Shan, S., Lü, X. 2017. Longan seed and mangosteen skin based activated carbons for the removal of Pb(II) ions and rhodamine-B dye from aqueous solutions. Desalin. Water Treat. 88, 154–161.

Hopkins, D., Hawboldt, K., 2020. Biochar for the removal of metals from solution: A review of lignocellulosic and novel marine feedstocks. J. Environ. Chem. Eng. 8, 103975.

Hou, Y., Yan, S., Huang, G., Yang, Q., Huang, S., Cai, J., 2020. Fabrication of N-doped carbons from waste bamboo shoot shell with high removal efficiency of organic dyes from water. Bioresour. Technol., 303, 122939.

Hu, C.-X., Zhou, J.-S., He, S., Luo, Z.-Y., Cen, K., 2009. Effect of chemical activation of an activated carbon using zinc chloride on elemental mercury adsorption. Fuel Proc. Technol., 90, 812–817.

Huang, X.-P., Yu, F., Peng, Q.-F., Huang, Y., 2018. Superb adsorption capacity of biochar derived from leather shavings for Congo red. RSC Adv. 8, 29781–29788.

Inyang, M., Gao, B., Zimmerman, A., Zhang, M., Chen, H., 2014. Synthesis, characterization, and dye sorption ability of carbon nanotube–biochar nanocomposites. Chem. Eng. J. 236, 39–46.

Islam, M.A., Ahmed, M.J., Khanday, W.A., Asif, M., Hameed, B.H., 2017. Mesoporous activated coconut shell-derived hydrochar prepared via hydrothermal carbonization-NaOH activation for methylene blue adsorption. J. Environ. Manag. 203, 237–244.

Jafari, A.J., Kakavandi, B., Kalantary, R.R., Gharibi, H., Asadi, A., Azari, A., Babaei, A.A., Takdastan, A., 2016. Application of mesoporous magnetic carbon composite for reactive dyes removal: Process optimization using response surface methodology. Korean J. Chem. Eng. 33, 2878–2890.

Jin, L., Zhao, X., Qian, X., Dong, M., 2018. Nickel nanoparticles encapsulated in porous carbon and carbon nanotube hybrids from bimetallic metal-organic-frameworks for highly efficient adsorption of dyes, J. Colloid Interf. Sci. 509, 245–253.

Jung, K.-W., Choi, B.H., Hwang, M.-J., Choi, J.-W., Lee, S.-H., Chang, J.-S., Ahn, K.-H., 2017. Adsorptive removal of anionic azo dye from aqueous solution using activated carbon derived from extracted coffee residues. J. Cleaner Prod. 166, 360–368.

Karcher, S., Kornmuller, A., Jekel, M., 2002. Anion exchange resins for removal of reactive dyes from textile wastewaters. Water Res. 36, 4717–4724.

Karimifard, S., Alavi Moghaddam, M.R., 2016. Removal of an anionic reactive dye from aqueous solution using functionalized multi-walled carbon nanotubes: isotherm and kinetic studies. Desalin. Water Treat. 57, 16643–16652.

Kelm, M.A.P., da Silva Júnior, M.J., de Barros Holanda, S.H., de Araujo, C.M.B., de Assis Filho, R.B., Freitas, E.J., dos Santos, D.R., da Motta Sobrinho, M.A., 2019. Removal of azo dye from water via adsorption on biochar produced by the gasification of wood wastes. Environ. Sci. Pollut. Res., 26, 28558–28573.

Khalil, K.M.S., Allam, O.A.S., Khairy, M., Mohammed, K.M.H., Elkhatib, R.M., Hamed, M. A., 2017. High surface area nanostructured activated carbons derived from sustainable sorghum stalk. J. Mol. Liquid. 247, 386–396.

Khraisheh, M.A.M., Al-Degs, Y.S., Allen, S.J., Ahmad, M.N., 2002. Elucidation of controlling steps of reactive dye adsorption on activated carbon. Ind. Eng. Chem. Res. 41, 1651–1657.

Kolur, N.A., Sharifian, S., Kaghazchi, T., 2019. Investigation of sulfuric acid-treated activated carbon properties. Turkish J. Chem. 43, 663–675.

Kyzas, G.Z., Deliyanni, E.A., Lazaridis, N.K., 2014. Magnetic modification of microporous carbon for dye adsorption. J. Colloid Interf. Sci. 430, 166–173.

Lambert, S.J., Davy, A.J., 2011. Water quality as a threat to aquatic plants: discriminating between the effects of nitrate, phosphate, boron and heavy metals on charophytes. New Phytol. 189, 1051–1059.

Langmuir, I., 1916. The constitution and fundamental properties of solids and liquids. J. Am. Chem. Soc. 38, 2221–2295.

Lawrence, C.W., 2014. High performance textiles and their applications. Woodhead Publishing, Cambridge, U.K.

Lawrinenko, M., Laird, D.A., 2015. Anion exchange capacity of biochar. Green Chem. 17, 4628–4636.

Lee, J.-W., Choi, S.-P., Thiruvenkatachari, R., Shim, W.-G., Moon, H., 2006. Evaluation of the performance of adsorption and coagulation processes for the maximum removal of reactive dyes. Dye. Pigm. 69, 196–203.

Lee, C.-Y.C., Pedram, E.O., Hines, A.L., 1986. Adsorption of oxalic, malonic, and succinic acids on activated carbon, J. Chem. Eng. Data 31, 133–136.

Li, D., Zhou, J., Wang, Y., Tian, Y., Wei, L., Zhang, Z., Qiao, Y., Li, J., 2019. Effects of activation temperature on densities and volumetric CO_2 adsorption performance of alkali-activated carbons. Fuel 238, 232–239.

Li, G., Zhu, W., Zhang, C., Zhang, S., Liu, L., Zhu, L., Zhao, W., 2016. Effect of a magnetic field on the adsorptive removal of methylene blue onto wheat straw biochar. Bioresour. Technol. 206, 16–22.

Li, H., Yang, S.-S., Sun, H., Liu, H., X.-H., 2018. Production of activated carbon from cow manure for wastewater treatment. Bioresour. 13, 3135–3143.

Li, N., Ma, X.-L., Zha, Q.-F., Kim, K.-S., Chen, Y.-S., Song, Y.-S., 2011. Maximizing the number of oxygen-containing functional groups on activated carbon by using ammonium persulfate and improving the temperature-programmed desorption characterization of carbon surface chemistry. Carbon 49, 5002–5013.

Li, W., Yang, K., Peng, J., Zhang, L., Guo, S., Xia, H., 2008. Effects of carbonization temperatures on characteristics of porosity in coconut shell chars and activated carbons derived from carbonized coconut shell chars. Ind. Crop. Prod. 28, 190–198.

Li, Y., Qi, J. W., Li, J. S., Shen, J. M., Liu, Y. X., Sun, X. Y., Shen, J. Y., Han, W. Q., & Wang, L. J., 2017. Nitrogen–doped hollow mesoporous carbon spheres for efficient water desalination by capacitive deionization. ACS Sust. Chem. Eng. 5, 6635–6644.

Li, Y., Li, Y., Zang, H., Chen, L., Meng, Z., Li, H., Ci, L., Du, Q., Wang, D., Wang, C., Li, H., Xia, Y., 2020. $ZnCl_2$–activated carbon from soybean dregs as a high–efficiency adsorbent for cationic dye removal: isotherm, kinetic, and thermodynamic studies. Environ. Technol. 41, 2013–2023.

Li, Y., Du, Q., Liu, T., Sun, J., Wang, Y., Wu, S., Wang, Z., Xia, Y., Xia, L., 2013. Methylene blue adsorption on graphene oxide/calcium alginate composites. Carbohydr. Polymer. 95, 501–507

Liang, X., Lu, Y., Li, Z., Yang, C., Niu, C., Su, X., 2017. Bentonite/carbon composite as highly recyclable adsorbents for alkaline wastewater treatment and organic dye removal. Micropor. Mesopor. Mater., 241, 107–114.

Liou, T.-H., 2010. Development of mesoporous structure and high adsorption capacity of biomass-based activated carbon by phosphoric acid and zinc chloride activation. Chem. Eng. J. 158, 129–142.

Liu, B., Gu, J., Zhou, J.-B., 2016. High surface area rice husk- based activated carbon prepared by chemical activation with $ZnCl_2$- $CuCl_2$ composite activator. Env. Prog. Sust. Energ. 35, 133–140.

Liu, J., Sun, N., Sun, C., Liu, H., Snape, C., Li, K., Wei, W., Sun, Y., 2015. Spherical potassium intercalated activated carbon beads for pulverized fuel CO_2 post-combustion capture. Carbon 94, 243–255.

Liu, X.-D., Tian, J.-F., Li, Y.-Y., Sun, N.-F., Mi, S., Xie, Y., Chen, Z., 2019. Enhanced dye adsorption from wastewater via Fe_3O_4 nanoparticles functionalized activated carbon, J. Hazard. Mater. 373, 397–407.

Liu, X., Sun, J., Duan, S. -X., Wang, Y., Hayat, T., Alsaedi, A., Wang, C.-M., Li, J.-X., 2017a. A valuable biochar from poplar catkins with high adsorption capacity for both organic pollutants and inorganic heavy metal ions. Sci. Rep. 7, 10033.

Liu, T., Li, Y., Peng, N., Lang, Q., Xia, Y., Gai, C., Zheng, Q., Liu, Z., 2017b. Heteroatoms doped porous carbon derived from hydrothermally treated sewage sludge: Structural characterization and environmental application. J. Environ. Manag. 197, 151–158.

Liu, T., Li, Y. H., Du, Q., Sun, J., Jiao, Y., Yang, G., Wang, Z., Xia, Y., Zhang, W., Wang, K., Zhu, H., Wu, D., 2012. Adsorption of methylene blue from aqueous solution by graphene. Colloid Surf. B 90, 197–203.

Liu, Y., Xu, H., Yang, X.-F, Tay, J.-H., 2003. A general model of biosorption of Cd^{2+}, Cu^{2+} and Zn^{2+} by aerobic granules. J. Biotechnol., 102, 233–239.

Long, Z., Zhan, Y., Li, F., Wan, X., He, Y., Hou, C., Hu, H., 2017. Hydrothermal synthesis of graphene oxide/multiwalled carbon nanotube/Fe_3O_4 ternary nanocomposite for removal of Cu (II) and methylene blue. J. Nanoparticle Res. 19, 318.

Low, K.S., Lee, C.K., 1997. Quaternized rice husk as sorbent for reactive dyes. Bioresour. Technol. 61, 121–125.

Lua, A.C., Yang, T., 2004. Effect of activation temperature on the textural and chemical properties of potassium hydroxide activated carbon prepared from pistachio-nut shell. J. Colloid Interf. Sci., 274, 594–601.

Machado, F.M., Bergmann, C.P., Fernandes, T.H.M., Lima, E.C., Royer, B., Calvete, T., Fagan, S.B., 2011. Adsorption of Reactive Red M-2BE dye from water solutions by multi-walled carbon nanotubes and activated carbon. J. Hazard. Mater. 192, 1122–1131.

Machado, F.M., Bergmann, C.P., Lima, E.C., Adebayo, M.A., Fagan, S.B., 2014. Adsorption of a textile dye from aqueous solutions by carbon nanotubes. Mater. Res. 17, 153–160.

Machado, F.M., Bergmann, C.P., Lima, E.C., Royer, B., De Souza, F.E., Jauris, I.M., Calvete, T., Fagan, S.B., 2012. Adsorption of Reactive Blue 4 dye from water solutions by carbon nanotubes: Experiment and theory. Phys. Chem. Chem. Phys. 14, 11139–11153.

Mahaninia, M.H., Rahimian, P., Kaghazchi, T., 2015. Modified Activated carbons with amino groups and their copper adsorption properties in aqueous solution. Chinese J. Chem. Eng., 23, 50–56.

Mahmoud, M.E., Nabil, G.M., El-Mallah, N.M., Bassiouny, H.I., Kumar, S., Abdel-Fattah, T.M., 2016. Kinetics, isotherm, and thermodynamic studies of the adsorption of reactive red 195 A dye from water by modified Switchgrass Biochar adsorbent. J. Ind. Eng. Chem. 37, 156–167.

Makhado, E., Pandey, S., Nomngongo, P.N., Ramontja, J., 2018. Preparation and characterization of xanthan gum-cl-poly(acrylic acid)/o-MWCNTs hydrogel nanocomposite as highly effective reusable adsorbent for removal of methylene blue from aqueous solutions. J. Colloid Interf. Sci. 513, 700–714.

Mao, B., Sidhureddy, B., Thiruppathi, A.R., Wood, P.C., Chen, A., 2020. Efficient dye removal and separation based on graphene oxide nanomaterials. New J. Chem. 44, 4519-4528.

Marrakchi, F., Bouaziz, M., Hameed, B.H., 2017a. Activated carbon–clay composite as an effective adsorbent from the spent bleaching sorbent of olive pomace oil: Process optimization and adsorption of Acid Blue 29 and methylene blue. Chem. Eng. Res. Design 128, 221–230.

Marrakchi, F., Auta, M., Khanday, W.A., Hameed, B.H., 2017b. High-surface-area and nitrogen-rich mesoporous carbon material from fishery waste for effective adsorption of methylene blue. Powder Technol. 321, 428–434.

Mohan, D., Singh, P., Sarswat, A., Steele, P.H., Pittman Jr, C.U., 2015. Lead sorptive removal using magnetic and nonmagnetic fast pyrolysis energy cane biochars. J. Colloid Interf. Sci. 448, 238–250

Mohan, D., Sarswat, A., Ok, Y., Pittman Jr, C.U., 2014. Organic and inorganic contaminants removal from water with biochar, a renewable, low cost and sustainable adsorbent – A critical review. Bioresour. Technol. 160, 191–202.

Moreno-Castilla, C., Ferro-Garcia, M.A., Joly, J.P., Bautista-Toledo, I., Carrasco-Marin, F., Rivera-Utrilla, J., 1995. Activated carbon surface modifications by nitric acid, hydrogen peroxide, and ammonium peroxydisulfate treatments. Langmuir 11, 4386–4392.

Nagano, S., Tamon, H., Adzumi, T., Nakagawa, K., Suzuki, T., 2000. Activated carbon from municipal waste. Carbon, 38, 915–920.

Nasrullah, A., Bhat, A.H., Naeem, A., Isa, M.H., Danish, M., 2018. High surface area mesoporous activated carbon-alginate beads for efficient removal of methylene blue. Int. J. Biologic. Macromol. 107, 1792–1799.

Nautiyal, P., Subramanian, K.A., Dastidar, M.G., 2016. Adsorptive removal of dye using biochar derived from residual algae after in-situ transesterification: Alternate use of waste of biodiesel industry. J. Environ. Manag. 182, 187–197.

Novak, J.M., Busscher, W.J., Laird, D.L., Ahmedna, M., Watts, D.W., Niandou, M.A.S., 2009. Impact of biochar amendment on fertility of a southeastern coastal plain soil. Soil Sci. 174, 105–112.

Oladipo, A.A., Ifebajo, A.O., Nisar, N., Ajayi, O.A., 2017. High-performance magnetic chicken bone-based biochar for efficient removal of Rhodamine-B dye and tetracycline: Competitive sorption analysis. Water Sci. Technol. 76, 373–385.

Osman, A.I., Blewitt, J., Abu-Dahrieh, J.K., Farrell, C., Al-Muhtaseb, A.H., J. Harrison, Rooney, D.W., 2019. Production and characterisation of activated carbon and carbon nanotubes from potato peel waste and their application in heavy metal removal. Environ. Sci. Pollut. Res. 26, 37228-37241.

Ōya, A., Marsh, H., 1982. Phenomena of catalytic graphitization. J. Mater. Sci. 17, 309–322.

Ozer, C., Imamoglu, M., 2017. Adsorptive transfer of methylene blue from aqueous solutions to hazelnut husk carbon activated with potassium carbonate. Desalination and Water Treat. 94, 236–243.

Özhan, A., Şahin, Ö., Küçük, M.M., Saka, C., 2014. Preparation and characterization of activated carbon from pine cone by microwave-induced $ZnCl_2$ activation and its effects on the adsorption of methylene blue. Cellulose **21,** 2457–2467.

Purkait, T., Singh, G., Singh, M., Kumar, D., Dey, R.S., 2017. Large area few-layer graphene with scalable preparation from waste biomass for high-performance supercapacitor. Sci. Rep. 7, 15239.

Qi, F.-J., Yan, Y., Lamb, D., Naidu, R., Bolan, N.S., Liu, Y.-J., Ok, Y.S., Donne, S.W., Semple, K.T., 2017. Thermal stability of biochar and its effect on cadmium adsorption. Bioresour. Technol. 246, 48–56.

Qian, L., Zhang, W., Yan, J., Han, L., Gao, W., Liu, R., Chen, M., 2016. Effective removal of heavy metal by biochar colloids under different pyrolysis temperatures. Bioresour. Technol. 206, 217–224.

Rajabi, M., Mahanpoor, K., Moradi, O., 2017. Removal of dye molecules from aqueous solution by carbon nanotubes and carbon nanotube functional groups: Critical review. RSC Adv. 7, 47083–47090.

Regti, A., Laamari, M. R., Stiriba, S.-E., El Haddad, M., 2017. Potential use of activated carbon derived from Persea species under alkaline conditions for removing cationic dye from wastewaters. J. Assoc. Arab Univ. Basic Appl. Sci. 24, 10–18.

Rodríguez, A., García, J., Ovejero, G., Mestanza, M., 2009. Adsorption of anionic and cationic dyes on activated carbon from aqueous solutions: Equilibrium and kinetics. J. Hazard. Mater. 172, 1311–1320.

Samarghandi, M.R., Hadi, M., Moayedi, S., Askari, F.B., 2009. Two-parameter isotherms of methyl orange sorption by pinecone derived activated carbon. Iranian J. Environ. Health Sci. Eng. 6, 285–294.

Shams, S.S., Zhang, L.S., Hu, R., Zhang, R., Zhu, J., 2015. Synthesis of graphene from biomass: A green chemistry approach. Mater. Lett. 161, 476–479.

Sangon, S., Hunt, A. J., Attard, T. M., Mengchang, P., Ngernyen, Y., Supanchaiyamat, N., 2018. Valorization of waste rice straw for the production of highly effective carbon-based adsorbents for dyes removal. J. Cleaner Prod. 172, 1128–1139.

Saroyan, H.S., Giannakoudakis, D.A., Sarafidis, C.S., Lazaridis, N.K., Deliyanni, E.A., 2017. Effective impregnation for the preparation of magnetic mesoporous carbon: application to dye adsorption. J. Chem. Technol. Biotechnol. 92, 1899–1911.

Sayğili, H., Güzel, F., 2018. Uptake of anionic and cationic dyes by highly effective porous carbon adsorber based on industrial processing residues. Separat. Sci. Technol. 53, 1465–1475.

Senthilkumaar, S., Kalaamani, P., Porkodi, K., Varadarajan, P.R., Subbhuraam, C.V., 2006. Adsorption of dissolved reactive dye from aqueous phase onto activated carbon prepared from agricultural waste. Bioresour. Technol. 97, 1618–1625.

Sevilla, M., Fuertes, A.B., 2010. Graphitic carbon nanostructures from cellulose. Chem. Phys. Lett. 490, 63–68.

Shabaan, O.A., Jahin, H.S., Mohamed, G.G., 2020. Removal of anionic and cationic dyes from wastewater by adsorption using multiwall carbon nanotubes. Arab. J. Chem. 13, 4797–4810.

Sharif, F., Gagnon, L.R., Mulmi, S., Roberts, E.P.L., 2017. Electrochemical regeneration of a reduced graphene oxide/magnetite composite adsorbent loaded with methylene blue. Water Res. 114, 237–245.

Sharma, Y.C., Uma, Gode, F., 2010. Engineering data for optimization of preparation of activated carbon from an economically viable material. Chem. Eng. Data 55, 3991–3994.

Shin, D.S., Kim, H.G., Ahn, H.S., Jeong, H.Y., Kim, Y.-J., Odkhuu, D., Tsogbadrakh, N., Lee, H.-B.-R., Kim, B.H., 2017. Distribution of oxygen functional groups of graphene

oxide obtained from low-temperature atomic layer deposition of titanium oxide. RSC Adv. 7, 13979–13984.

Shirzad-Siboni, M., Khataee, A., Joo, S.W., 2014. Kinetics and equilibrium studies of removal of an azo dye from aqueous solution by adsorption onto scallop. J. Ind. Eng. Chem. 20, 610–615.

Silva, T.L., Cazetta, A.L., Souza, P.S.C., Zhang, T., Asefa, T., Almeida, V.C., 2018. Mesoporous activated carbon fibers synthesized from denim fabric waste: Efficient adsorbents for removal of textile dye from aqueous solutions. J. Cleaner Prod. 171, 482–490.

Silva, T.L., Ronix, A., Pezoti, O., Souza, L.S., Leandro, P.K.T., Bedin, K.C., Beltrame, K. K., Cazetta, A.L., Almeida, V.C., 2016. Mesoporous activated carbon from industrial laundry sewage sludge: Adsorption studies of reactive dye Remazol Brilliant Blue R. Chem. Eng. J. 303, 467–476.

Soares, A., Guieysse, B., Jefferson, B., Cartmell, E., Lester, J.N., 2008. Nonylphenol in the environment: A critical review on occurrence, fate, toxicity, and treatment in wastewaters. Environ. Int. 34, 1033–1049.

Sonai, G.G., de Souza, S.M.A.G.U., de Oliveira, D., de Souza, A.A.U., 2016. The application of textile sludge adsorbents for the removal of Reactive Red 2 dye. J. Environ. Manag. 168, 149–156.

Sun, D., Zhang, Z., Wang, M., Wu, Y., 2013. Adsorption of reactive dyes on activated carbon developed from Enteromorpha prolifera. Am. J. Anal. Chem. 4, 17–26.

Tessmer, C.H., Vidic, R.D., Uranowski, L.J., 1997. Impact of oxygen-containing surface functional groups on activated carbon adsorption of phenols. Environmental Sci. Technol. 31, 1872–1878.

Thitame, P.V., Shukla, S.R., 2016. Adsorptive removal of reactive dyes from aqueous solution using activated carbon synthesized from waste biomass materials. International J. Environ. Sci. Technol. 13, 561–570.

Tran, H.N., Chao, H.-P., You, S.-J., 2018. Activated carbons from golden shower upon different chemical activation methods: Synthesis and characterizations. Adsorption Sci. Technol. 36, 95–113.

Tran, H.N., Huang, F.-C., Lee, C.-K., Chao, H.-P., 2017. Activated carbon derived from spherical hydrochar functionalized with triethylenetetramine: Synthesis, characterizations, and adsorption application. Green Process. Synth. 6, 565–576.

Travlou N.A., Kyzas G.Z., Lazaridis N.K., Deliyanni E.A., 2013. Graphite oxide/chitosan composite for reactive dye removal. Chem. Eng. J. 217, 256–265.

Tuzen, M., Sari, A., Saleh, T.A., 2018. Response surface optimization, kinetic and thermodynamic studies for effective removal of rhodamine B by magnetic AC/CeO_2 nanocomposite. J. Environ. Manag. 206, 170–177.

Üner, O., Bayrak, Y., 2018. The effect of carbonization temperature, carbonization time and impregnation ratio on the properties of activated carbon produced from *Arundo donax*. Micropor. Mesopor. Mater. 268, 225–234.

Vijayaraghavan, K., Padmesh, T.V.N., Palanivelu, K., Velan, M., 2006. Biosorption of nickel(II) ions onto *Sargassum wightii*: application of two-parameter and three-parameter isotherm models. J. Hazard. Mater. B133, 304–308.

Wang, G., Wang, S., Sun, W., Sun, Z., Zheng, S., 2017. Oxygen functionalized carbon nanocomposite derived from natural illite as adsorbent for removal of cationic and anionic dyes. Adv. Powder Technol. 28, 1943–1953.

Wang, J., Heerwig, A., Lohe, M.R., Oschatz, M., Borchardt, L., Kaskel, S., 2012. Fungi-based porous carbons for CO_2 adsorption and separation. J. Mater. Chem. 22, 13911–13913.

Weber, K., Quicker, P., 2018. Properties of biochar. Fuel 217, 240–261.

Wu, Y., Cha, L., Fan, Y., Fang, P., Ming, Z., Sha, H., 2017. Activated biochar prepared by pomelo peel using H_3PO_4 for the adsorption of hexavalent chromium: performance and mechanism. Water, Air, Soil, Pollut. 228, 405.

Xie, X., Goodell, B., Qian, Y., Daniel, G., Zhang, D., Nagle, D.C., Peterson, M.L., Jellison, J., 2009. A method for producing carbon nanotubes directly from plant materials. Forest Prod. J. 59, 26–28.

Xu, S.-S., Qiu, S.-W., Yuan, Z.-Y., Ren, T.-Z., Bandosz, T.J., 2019. Nitrogen-containing activated carbon of improved electrochemical performance derived from cotton stalks using indirect chemical activation. J. Colloid Interf. Sci. 540, 285–294.

Yagub, M.T., Sen, T.K., Afroze, S., Ang, H.M., 2014. Dye and its removal from aqueous solution by adsorption: A review. Adv. Colloid. Interf. Sci. 209, 172–184.

Yakout, A.A., Shaker, M.A., 2016. Dodecyl sulfate functionalized magnetic graphene oxide nanosheet for the investigation of fast and efficient removal of aqueous malachite green. J. Taiwan Inst. Chem. Eng. 63, 81–88

Yakout, S.M., El-Deen, G.S., 2016. Characterization of activated carbon prepared by phosphoric acid activation of olive stones. Arabian J. Chem. 9, S1155–S1162.

Yang, K., Li, X., Cui, J., Zhang, M., Wang, Y., Lou, Z., Shan, W., Xiong, Y., 2020. Facile synthesis of novel porous graphene-like carbon hydrogel for highly efficient recovery of precious metal and removal of organic dye. Appl. Surf. Sci. 528, 146928.

Yang, Y., Lin, X., Wei, B., Zhao, Y., Wang, J., 2014. Evaluation of adsorption potential of bamboo biochar for metal-complex dye: equilibrium, kinetics and artificial, neural network modeling. Int. J. Environ. Sci. Technol. 11, 1093–1100.

Yuan, J.-H., Xu, R.-K., 2017. The amelioration effects of low-temperature biochar generated from nine crop residues on an acidic Ultisol. Soil Use Manag. 27, 110–117.

Zambare, R., Song, X., Bhuvana, S., Antony Prince, J.S., Nemade, P., 2017. Ultrafast dye removal using ionic liquid graphene oxide sponge. ACS Sust. Chem. Eng. 5, 6026–6035.

Zhang, C., Lin, S., Peng, J., Hong, Y., Wang, Z., Jin, X., 2017. Preparation of highly porous carbon through activation of NH_4Cl induced hydrothermal microsphere derivation of glucose. RSC Adv. 7, 6486–6491.

Zhang, W., Yang, Q., Luo, Q., Shi, L., Meng, S., 2020. Laccase-Carbon nanotube nanocomposites for enhancing dyes removal. J. Cleaner Prod. 242, 118425.

Zheng, X., Huang, M., You, Y., Fu, X., Liu, Y., Wen, J., 2018. One-pot synthesis of sandwich-like MgO@Carbon with enhanced sorption capacity of organic dye. Chem. Eng. J. 334, 1399–1409.

Zheng, Y., Chen, D., Li, N., Xu, Q., Li, H., He, J., Lu, J., 2017. Highly efficient simultaneous adsorption and biodegradation of a highly concentrated anionic dye by high-surface-area carbon-based biocomposites. Chemosphere 179, 139–147.

Zhou, X., Wang, P., Zhang, Y., Wang, L., Zhang, L., Zhang, L., Xu, L., Liu, L., 2017. Biomass based nitrogen-doped structure-tunable versatile porous carbon materials. J. Mater. Chem. A 5, 12958–12968.

Declaration of Interest Statement

Figure

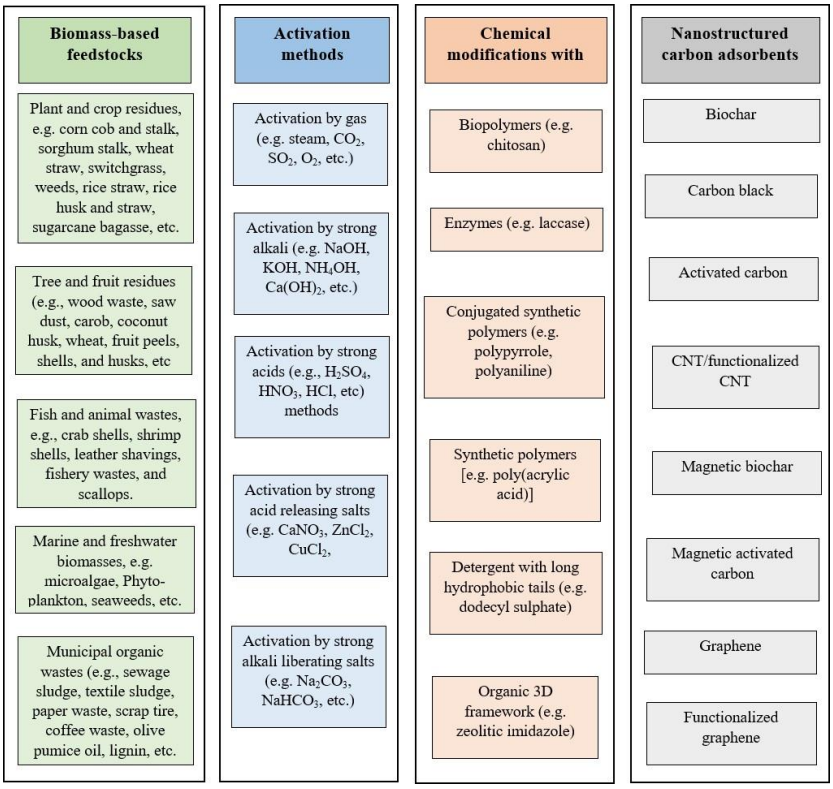

Fig. 1.

Figure


Dried feedstocks
Carbonisation in air
600–1200 °C
Charcoal
Physical activation With steam/O_2/ CO_2/SO_2
Activation
Chemical activation with acid/alkali/ their salt
Activated carbon
Grinding
GAC
PAC

Fig. 2.

Figure

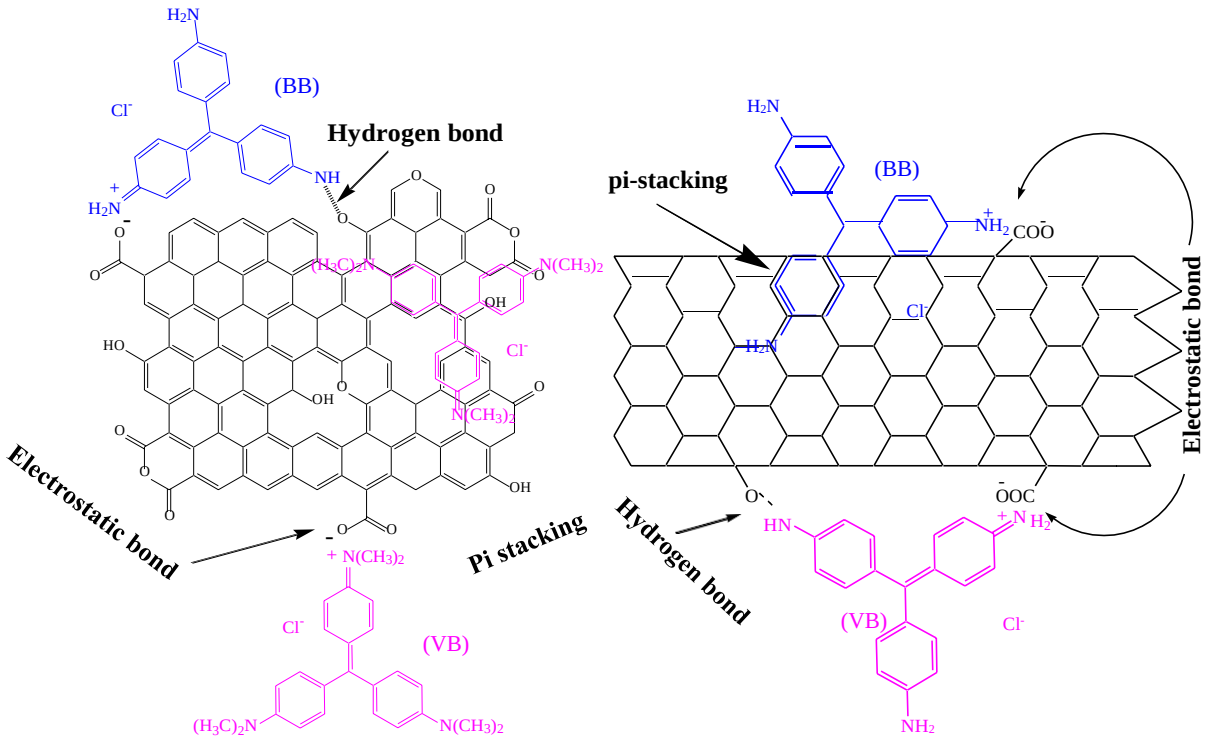
(BB)
Hydrogen bond
Electrostatic bond
Pi stacking
(VB)
pi-stacking
Hydrogen bond
Electrostatic bond
(BB)
(VB)

Fig. 3.

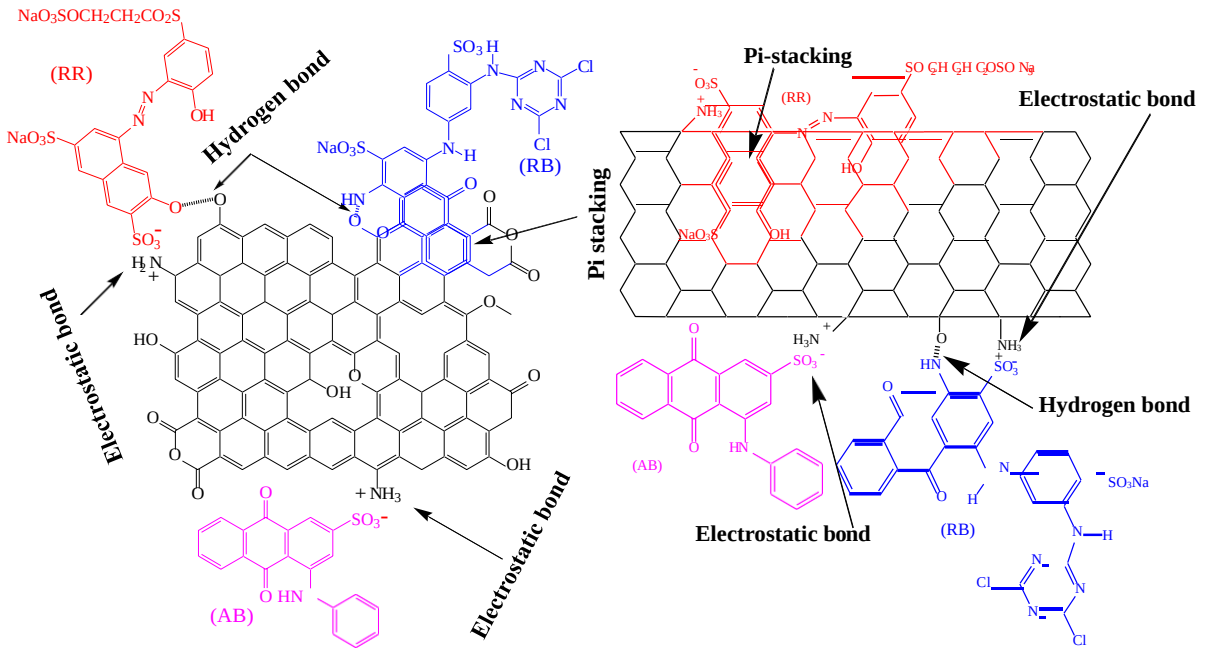
(RR)
(RB)
(AB)
Hydrogen bond
Electrostatic bond
Pi stacking
Pi-stacking
Electrostatic bond
Electrostatic bond
Hydrogen bond

Fig. 4.

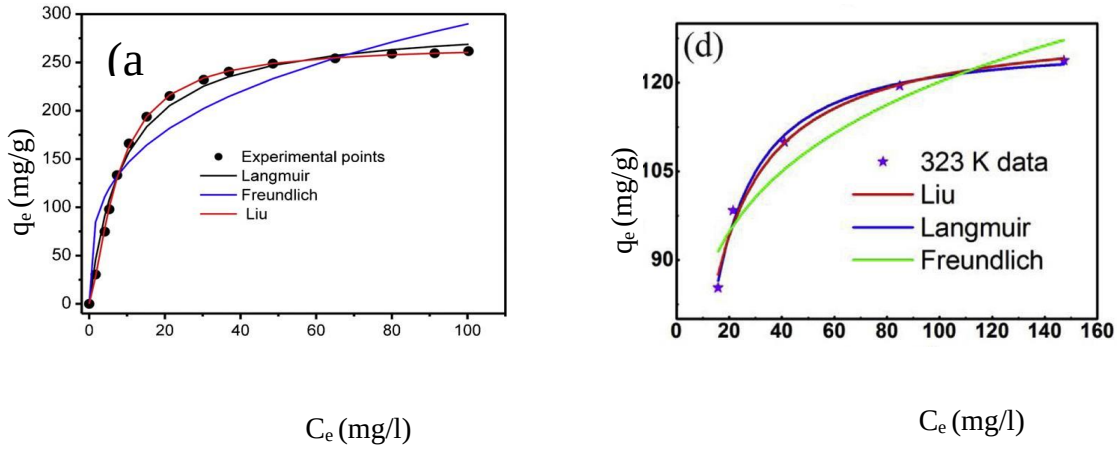
(a
Experimental points
Langmuir
Freundlich
Liu
qe (mg/g)
Ce (mg/l)
(d)
323 K data
Liu
Langmuir
Freundlich
qe (mg/g)
Ce (mg/l)

Fig. 5.

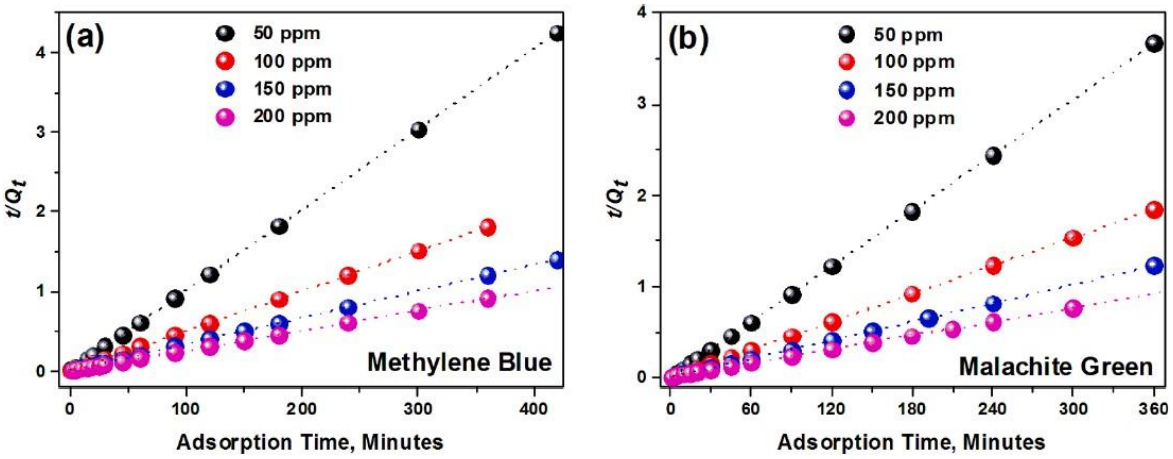
(a)
50 ppm
100 ppm
150 ppm
200 ppm
Methylene Blue
t/Qt
Adsorption Time, Minutes
(b)
50 ppm
100 ppm
150 ppm
200 ppm
Malachite Green
t/Qt
Adsorption Time, Minutes

Fig. 6.

Table 1.

Absorption conditions and adsorption capacity of various anionic dyes by biochar derived from various feedstocks.

Feedstocks	Dye type	Treatment methods	BET Surface area of carbon (m^2/g)	Operating conditions						Absorption capacity (mg/g)	Ref.
				Temp. of treatment (°C)	Optimum pH	Dosage of sorbent (g/L)	Agitation speed (rpm)	Dye conc. (mg/L)	Contact time (min)		
Ashe Juniper	C.I. Basic Blue 9	Batch	433–511	25	6.0	0.5	200	550	4320	420.86	Choi et al., 2019
Pinecone	C.I. Basic Blue 9	Batch	335	35	11.3	0.4	–	10–70	210	106.4	Dawood et al., 2017
Cassava	C.I. Basic Green 4	Batch	2.38	25	4.0	0.05	300	150	120	933.00	Beakou et al., 2017a
Wheat straw biochar	C.I. Basic Blue 9	Batch	n/a	25	11.0	0.5	n/a	10–100	1440	46.6	Li et al., 2016
Wheat straw biochar under magnetic field										62.5	
Switchgrass	Reactive Red 195A	Batch		25±1	7	1	150	90	30	1288.4	Mahmoud et al., 2016
Corn cob	C.I. Basic Blue 9	Batch	-	25						126.58	Fang, 2012
	C.I. Basic Violet 3									81.96	
	C.I. Basic Red 9									75.18	
Wood waste	C.I. Direct Black 22	Batch	350.4	28	2.0	4.0	200	50	180	185	Kelm et al., 2019
Crab shell	C.I. Basic Green 4	Batch	81.57	25	7.0	0.5	-	6000	350	12502	Dai et al., 2018
	C.I. Direct Red 28				4.0			1500		20317	
Weeds	C.I. Basic Blue 9	Batch	40.46	50	7.4	2.0	120	100	480	39.7	Güzel et al, 2017
Oxidized weeds			17.56							161.3	
Spirulina platensis algae	C.I. Direct Red 28	Batch	-		2.0	2.0	-	90		37.17	Nautial et al., 2016
Leather shavings	C.I. Direct Red 28	Batch	2365	30	8.0	0.4	-	900	1440	1916.56	Hunag et al., 2018
Bamboo	C.I. Acid Black 170	Batch	517.28	30	1.0	0.4	200	500	480	215.50	Yang et al., 2014
Poplar Catkins	C.I. Basic Blue 9	Batch	351.4	30	6.0	0.04	-	60	1440	534.00	Liu et al., 2017b
	C.I. Acid Orange 52									154.00	
	C.I. Direct Red 28									350	
Coconut shell	C.I. Basic Blue 9	Batch	876.14	30	7.0	1.0	120	100	1500	200	Islam et al., 2017

Table 2.

Dye-binding performance of various modified/composite carbonaceous adsorbents studied by the batch process.

Adsorbents	Dye type	Operating conditions						Dye-binding capacity (mg/g)	Ref.
		Temp. (°C)	Optimum pH	Dosage of sorbent (mg/l)	Agitation speed (rpm)	Dye conc. (mg/l)	Contact time (min)		
CNT/bagasse biochar composite	C.I. Basic Blue 9	22±0.5	7.0	2.0	-	20	1440	6.2	Inyang et al., 2014
Chitosan/ Graphene Oxide Composite	C.I. Reactive Red 120	60	3	2.8	n/a	100	480	32.2	Guo et al., 2016
	C.I. Reactive Black 5	25 45 65	2	1	160	300	1440	277.0 377.0 425.0	Travlou et al., 2013
Graphene oxide/calcium alginate composite	C.I. Basic Blue 9	25	7	2.0	n/a	30-80	300	181.8	Li et al., 2013
Xanthan gum-cl-poly(acrylic acid)/oxidized-MWCNTs hydrogel nanocomposite	C.I. Basic Blue 9	30	7	2.5	180	200	120	521.0	Guo et al., 2018
MgO/carbon nanocomposites	C.I. Acid Orange 52	20	10.2	0.75	n/a	70	180	101.4	Zheng et al., 2018
Mesoporous activated carbon-alginate beads	C.I. Basic Blue 9	25	8	0.333	n/a	100	1440	230.6	Nasrullah et al., 2018
Nickel nanoparticles encapsulated in porous carbon and carbon nanotube hybrids	C.I. Basic Green 4	n/a	n/a	0.25	n/a	20-350	60	898.0	Jin et al., 2018
	C.I. Direct Red 28							818.0	
	C.I. Basic Violet 10							395.0	
	C.I. Basic Blue 9							312.0	
	C.I. Acid Orange 52							271.0	
Ionic Liquid-Graphene Oxide Sponge	C.I. direct Red 80	23	2.0	0.1–1.0	150	25–100	90	501.3	Zambare et al., 2017
Heteroatom-doped porous carbon	C.I. Acid Orange 7	25	n/a	1.0	n/a	40-360	25	440.5	Liu et al., 2017
AC immobilized on chitosan beads	C.I. Basic Violet 10		6	0.1	150	10–2000	1440–4320	50.7	Filipkowska et al., 2017
	C.I. Reactive Black 5		4					639.8	
GO-zeolitic imidazolate framework	C.I. Basic Green 4	20	7	0.018	600	50	240	3300.0	Abdi et al., 2017
CNT-zeolitic imidazolate framework				0.031				2034.0	
AC/bentonite composites	C.I. Basic Blue 9	25		0.1	160	20	65	270.1	Liang et al., 2017
AC /bentonite/ lime	C.I. Reactive Blue 19	25	2	1	200	200	120	110.6	
N-doped AC derived from	C.I. Basic Violet 10	25	-	1.0	-	2-300	300	140.0	Hou et al., 2020
	C.I. Acid Orange 52							100.0	

N-doped AC derived from functionalized cresol	C.I. Basic Violet 10	-	-	0.12	500	25	1440	204.1	El-Mahdy et al., 2010
	C.I. Basic Blue 9							308.6	
CNT/chitosan hydrogel	C.I. Acid Blue 9	25	3	-	50	50-400	1440	1508.5	Gonçalves et al., 2020
	C.I. Acid Red 40	55						1482.3	
Zn-doped AC	C.I. Acid Blue 9	50	-	-	-	-	-	255.1	Li et al., 2020
Graphene-like carbon hydrogel	C.I. Basic Blue 9	30	4	1.0	-	20	240	13381.62	Yang et al., 2020
Laccase-modified-CNT	C.I. Acid Orange 7			0.08	250	10-60	180	86.0	Zhang et al., 2020
Fe-La modified AC	C.I. Basic Blue 9	30	n/a	1.0	300	200–600	60	261.1	Cheng et al., 2017
Hydrochar functionalized-TETA	C.I. Basic Green 5	30	5.0	4.0	180	100–1000	2880	175.0	Tran et al., 2017
Zeolite/AC composites	C.I. Basic Blue 9	25	-	0.11	-	595	-	754.75	Wang et al., 2018
AC/polyaniline	C.I. Acid Orange 52	-	6.5	1440	200	20-120	1440	285	Hasan et al., 2019

Table 3

Absorption of anionic and cationic dyes by magnetic AC adsorbents studied by the batch process.

Adsorbents	Dye type	Operating conditions						Absorption capacity (mg/g)	Ref.
		Temp. of treatment (°C)	Optimum pH	Dosage of sorbent (g/L)	Agitation speed (rpm)	Dye conc. (mg/L)	Contact time (min)		
Mesoporous AC/Fe_3O_4	C.I. Reactive Black 5	25	10.0	0.5	140	250–1300	4320	445.3	Saroyan et al., 2017
GO/MWCNT/ Fe_3O_4	C.I. Basic Blue 9	25±1	9.0	0.5	n/a	10-90	1440	69.4	Long et al., 2017
rGO/ Fe_3O_4	C.I. Basic Blue 9	25	n/a	0.5	n/a	25	60	39.0	Sharif et al., 2017
CNT/carrageenan/ Fe_3O_4	C.I. Reactive Black 5	25	2	0.4	150	19.84	1440	29.6	Duman et al., 2016
Biochar/Fe_3O_4	C.I. Mordant Black 11	25	3.4	2.3	-	50	50	27.85	Akbarnezhad and Safa, 2018
CBD biochar/Fe_3O_4	C.I. Basic Violet 10	26±2	10	10	150	100	1440	96.5	Oladipo et al., 2017
RHD biochar/Fe_3O_4	C.I. Acid Orange 52	25.0	4.06	0.6	-	60	30	98.5	Han et al., 2015
Graphene/PPy/Fe_3O_4	C.I. Basic Blue 9	30	7	0.33	150	100-200	60	270.3	Bai et al., 2015
CO-f-GO/ Fe_3O_4	C.I. Basic Violet 10	25		0.132	n/a	5	200	36.0	Guo et al., 2018
GO/Fe_3O_4	C.I. Basic Blue 9			0.07		10		21.0	
DDS-f-GO/Fe_3O_4	C.I. Basic Green 4	25	7.0	0.04-2.0	n/a	25	60	714.3	Yakout and Shaker, 2016
PAC/Fe_3O_4	C.I. Reactive Black 5	25± 1	4±0.50	1.5	200	150	n/a	175.4	Jafari et al., 2016
	C.I. Reactive Red 120	35						172.4	
AC/Fe_3O_4	C.I. Reactive Black 5	25	10	0.8	160	100	3000	54.8	Kyzas et al., 2014
AC-NS/Fe_3O_4	C.I. Acid Blue 90	-	2	0.03	50	80	180	78.25	Abdel-Ghani et al., 2019

Table 4.

Chemical structure and molecular weight of several basic and reactive dyes.

Name of dye	Chemical structure	Molecular weight (g/mol)
C.I. Reactive Blue 2	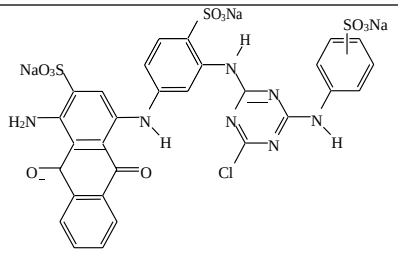	840.11
C.I. Reactive Yellow 2	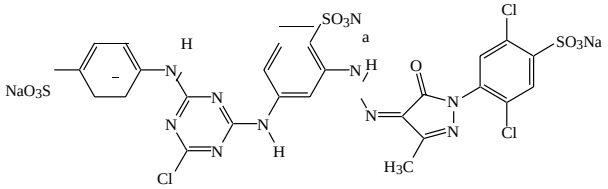	872.97
C.I. Reactive Blue 4	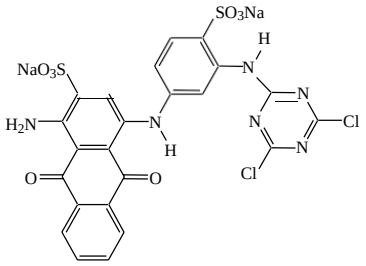	681.39
C.I. Reactive Blue 171	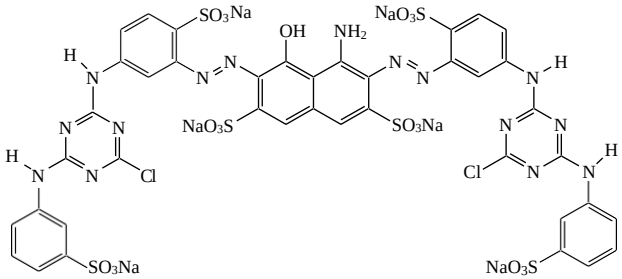	1418.93
C.I. Reactive Red 23	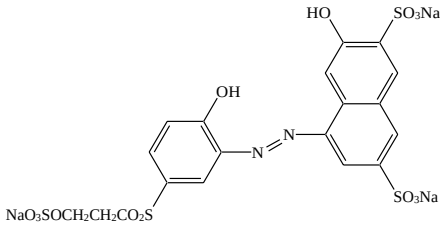	678.53

C.I. Reactive Red 2	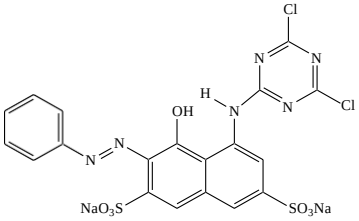	615.34
C.I. Reactive Yellow 145	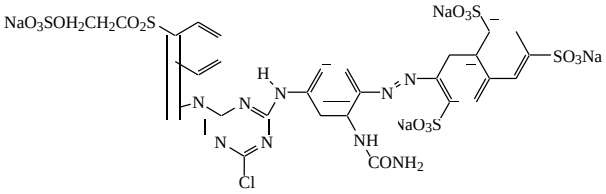	1026.25
C.I. Basic Blue 9	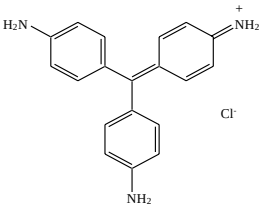	373.89
C.I. Basic Violet 3	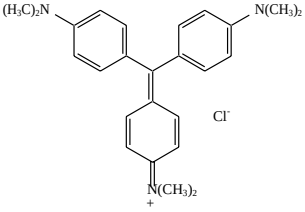	407.98